Journal of Hazardous Materials 446 (2023) 130669

Contents lists available at ScienceDirect

Journal of Hazardous Materials

journal homepage: www.elsevier.com/locate/jhazmat

Research Paper

Chitosan oligosaccharide alleviates and removes the toxicological effects of organophosphorus pesticide chlorpyrifos residues

Huiyang Fu [a,c], Haozhen Liu [a], Yao Ge [b], Yinfeng Chen [a], Peng Tan [a], Jun Bai [a], Zhaolai Dai [a], Ying Yang [a,*], Zhenlong Wu [a,b,c]

[a] State Key Laboratory of Animal Nutrition, Department of Companion Animal Science, China Agricultural University, Beijing 100193, China
[b] Beijing Advanced Innovation Center for Food Nutrition and Human Health, China Agricultural University, Beijing 100193, China
[c] Beijing Jingwa Agricultural Science and Technology Innovation Center, #1, Yuda Road, Pinggu, Beijing 101200, China

HIGHLIGHTS

- Chlorpyrifos (CHP) residues caused the decrease in productive performance on rats.
- The mechanism of CHP to intestinal toxicity is explored.
- Chitosan oligosaccharide (COS) can alleviate the CHP-induced toxicological effects.
- COS can effectively improve CHP-induced intestinal metabolic dysfunction on rats.

GRAPHICAL ABSTRACT

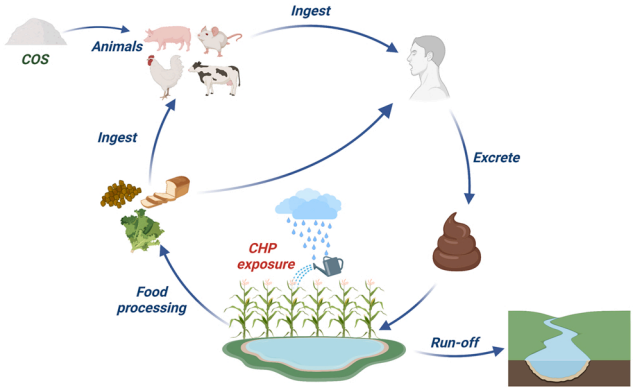

Abbreviations: CHP, Chlorpyrifos; OPPs, Organophosphorus pesticides; WHO, World Health Organization; AChE, Acetylcholinesterase; ROS, Reactive oxygen species; COS, Chitosan oligosaccharide; IF, Immunofluorescence; IW, Initial weight; FW, Final weight; ADG, Average daily gain; ADFI, Average daily feed intake; ELISA, Enzyme-linked immunosorbent assay; ALB, Albumin; AKP, Alkaline phosphatase; ALT, Alanine aminotransferase; AST, Aspartate aminotransferase; TBIL, Total bilirubin; DBIL, Direct bilirubin; CRE, Creatinine; BUN, Blood urea nitrogen; URIC, Uric acid; ACh, Acetylcholine; T-AOC, Total antioxidant capacity; T-SOD, Total superoxide dismutase; SOD1, Superoxide dismutase, soluble; SOD2, Superoxide dismutase in mitochondrial; GPx, Glutathione peroxidase; GPx1, Glutathione peroxidase cytoplasm; GST, Glutathione S-transferase; CAT, Catalase; H_2O_2, Hydrogen peroxide; MDA, Methane dicarboxylic aldehyde; Keap1, Kelch-like ECH-associated protein; Nrf2, Nuclear factor erythroid 2-related factor 2; HO-1, Heme oxygenase 1; HE, Hematoxylin-eosin; IL-1β, Interleukin-1β; IL-6, Interleukin-6; IL-10, Interleukin-10; TNF-α, Tumour necrosis factor-α; GCLC, Glutamate cysteine ligase catalyses subunit; GCLM, Glutamic acid cysteine ligase modified subunit; INF-γ, γ-interferon; NF-κB, Nuclear factor kappa B; V/C, Villi to crypt ratio; ZO-1, Zona occludin-1; PBS, Phosphate buffered saline; LSCM, Laser scanning confocal microscopy; DAPI, 4',6-diamidino-2-phenylindole; TUNEL, Terminal deoxynucleotidyl transferase-mediated dUTP nick-end labelling; Bcl-2, B-cell lymphoma-2; Bad, Bcl2 associated death promoter; Bax, Bcl2-associated X; qRT-PCR, Quantitative real-time polymerase chain reaction; GAPDH, Glyceraldehyde-3-phosphate dehydrogenase; BCA, Bicinchoninic acid; SDS-PAGE, Sodium dodecyl sulphate polyacrylamide gel electrophoresis; PVDF, Polyvinylidene fluoride; BSA, Bovine albumin; ANOVA, Analysis of variance; TLRs, Toll-like receptors; PCA, Principal component analysis; PLS-DA, Partial least-squares discriminant analysis; ORA, Over-representation analysis; KEGG, Kyoto Encyclopedia of Genes and Genomes; OTUs, Operational taxonomic units; NMDS, Non-metric multidimensional scaling; PCoA, Principal coordinate analysis; LEfSe, Linear discriminant analysis effect size; LDA, Linear discriminant analysis; RDA, Redundancy analysis; AChRs, ACh receptors; MRs, Muscarinic receptors; GI, Gastrointestinal; 5-HT, 5-hydroxytryptamine; SCFAs, Short-chain fatty acids.

* Correspondence to: State Key Laboratory of Animal Nutrition, China Agricultural University, Beijing 100193, China.
E-mail address: cauvet@163.com (Y. Yang).

https://doi.org/10.1016/j.jhazmat.2022.130669
Received 17 September 2022; Received in revised form 4 December 2022; Accepted 23 December 2022
Available online 24 December 2022

ARTICLE INFO

Editor: Dr. S Nan

Keywords:
Environmental contaminant
Toxicological effects
Remove
Organophosphorus pesticides
Chlorpyrifos

ABSTRACT

The abuse of chlorpyrifos (CHP), a commonly used organophosphorus pesticide, has caused many environmental pollution problems, especially its toxicological effects on non-target organisms. First, CHP enriched on the surface of plants enters ecosystem circulation along the food chain. Second, direct inflow of CHP into the water environment under the action of rainwater runoff inevitably causes toxicity to non-target organisms. Therefore, we used rats as a model to establish a CHP exposure toxicity model and studied the effects of CHP in rats. In addition, to alleviate and remove the injuries caused by residual chlorpyrifos *in vivo*, we explored the alleviation effect of chitosan oligosaccharide (COS) on CHP toxicity in rats by exploiting its high water solubility and natural biological activity. The results showed that CHP can induce the toxicological effects of intestinal antioxidant changes, inflammation, apoptosis, intestinal barrier damage, and metabolic dysfunction in rats, and COS has excellent removal and mitigation effects on the toxic damage caused by residual CHP in the environment. In summary, COS showed significant biological effects in removing and mitigating blood biochemistry, antioxidants, inflammation, apoptosis, gut barrier structure, and metabolic function changes induced by residual CHP in the environment.

1. Introduction

Chlorpyrifos [O, O-diethyl-O-(3,5,6-trichloro-2-pyridyl) phosphorothioate; CHP] is the fourth most widely used pesticide worldwide after monocrotophos, acephate, and endosulfan and is the most frequently detected organophosphorus insecticide [1,2]. According to the World Health Organization (WHO) classification of organophosphorus pesticides (OPPs), CHP is a moderately toxic class II pesticide; thus, it is relatively safe compared with other OPPs, which has led to its indiscriminate use and abuse in agricultural production [3]. Currently, CHP is widely used in agriculture, industrial sites, household pesticides, horticulture, and government as a nematicide and acaricide to control various crops, lawns, and ornamental plants [4,5]. China alone used more than 2000 tons of CHP in 2014, and in the past decade, its use in Brazil reached 570 million litres [6,7]. By 2018, the total use of CHP in China was 28,600 tons [2]. The amount acting on the intended target after CHP application is less than 0.1%, and the remainder remains in the environment [8]. Residual and non-target CHP enter ecosystem circulation through rainwater runoff, accumulate in river water, soil, and the atmosphere, and are then taken up by non-target organisms. CHP has been widely detected in the water environment of agricultural areas during the plant growing season [9]. CHP residues have also been detected in common crops such as tomato, organic spinach, apple, and soybean [10–13]. In addition, because of the strong hydrophobicity of CHP, its half-life in the environment can exceed 2 years [14,15]. This resulted in a detection rate of 54% in all surface water samples [16]. Residual CHP in food is also stable during storage and can even be detected in processed products [17]. For example, after 120 days of storage, the residue in wheat reached 28%. CHP residues in flour, chapattis, and bread after processing reached 65–83%, 29–51%, and 25–75%, respectively [18]. After kneading, fermentation, and steaming, CHP residues in Chinese steamed buns can only be reduced by 36%, 5%, and 4–38%, respectively [19]. These residues eventually lead to CHP enrichment in humans and animals through food, drinking water, and direct contact with the skin [20]. For example, CHP and its metabolites have been detected in the urine of pregnant women [21]. CHP use peaked in the 1960 s, followed by approximately 278 documented cases of human CHP poisoning between 1974 and 2005 [22]. Therefore, in 2000, the US Environmental Protection Agency proposed stopping the use of CHP, which restricted and banned its application in many countries to ensure environmental safety and animal health [13,23].

The gut is the first physiological barrier to exposure to the environmental pollutant CHP after ingestion [24]. Breakdown of the intestinal barrier may affect digestion and absorption of nutrients by humans and animals. After CHP is absorbed in the intestines, it is detoxified into 3,5,6-trichloro-2-pyridinol and the active substance CHP-oxon under the action of cytochrome P450 in vivo [25]. The latter blocks the cholinergic pathway of nerve cells by irreversibly inhibiting the activity of acetylcholinesterase (AChE) [26]. Oxidative stress is also a major toxicity mechanism during chronic and subchronic CHP exposure [27]. CHP can cause neuronal damage through increased production of reactive oxygen species (ROS), DNA damage, and lipid peroxidation, resulting in deficits in motor activity, cognitive performance, and coordination skills [28]. In addition, toxicity of CHP to other systems has also been reported, including reduced male reproductive capacity [29] and hepatotoxicity [30]. Long-term exposure to CHP can also lead to impaired fertility, hatchability, and embryo deformities [31]. CHP exposure can affect the foetal nervous system, thereby causing neurological damage in new-borns [32]. However, the toxicological effects of CHP on gut health have not been reported, and after oral administration, intestinal absorption is the main route by which environmental residual CHP enters the body. Therefore, the effect of CHP on gut health is of particular concern.

Therefore, we used rats as the research object [33] to establish a poisoning model to evaluate the toxicological effects of CHP residues in the environment on the gut. The toxicity of CHP to organisms and its molecular mechanisms were evaluated from the aspects of small intestine antioxidant capacity, inflammation, apoptosis, intestinal integrity, intestinal metabolic function, and microbial abundance. In addition, chitosan oligosaccharide (COS) is an oligomer with high water solubility and biological activity that maintains significant natural biological activity [34]. It may have the potential to improve immunity and regulate the metabolism of toxins [35,36]. Moreover, COS exhibits biological activity that promotes growth [37,38], improves intestinal morphology and barrier function [39–42], enhances intestinal structure [43], and improves antioxidant capacity and immunity [41,44]. COS is also involved in scavenging intracellular free radicals, significantly inhibiting the activation of NF-*k*B, effectively enhancing systemic immune responses, and regulating the function of immunoreactive cells [45]. Based on these positive effects, we further hypothesised whether COS could effectively remove and mitigate the toxicological effects of the exogenous pollutant CHP on intestines. Our findings support the idea that COS has a significant effect on removing and mitigating the toxicity caused by residual CHP in the environment. In the present experiment, we used COS to alleviate the toxic effects caused by CHP and explored the related mechanisms for the first time. Furthermore, 16S rRNA sequencing and metabolomics were used to investigate the CHP-induced intestinal metabolite and microbial changes in rats and the mitigating effects of COS. Finally, compared to previous experiments, we added Spearman correlation analysis to predict the possible role of gut microbes in intestinal metabolic pathways [24,46–48]. These results offer new prospects for the prevention and treatment of CHP.

2. Materials and methods

2.1. Experimental design and feeding management

A total of 32 female SD rats with bodyweights ranging from 180 to 200 g purchased from Beijing Huafukang Bioscience Co., Ltd. (Beijing, China) were selected for the experiment. A 7-day pre-experimentation period was performed before the start of the experiment, and the formal test began after the end of the pre-experimentation period. The experiment adopted a 2 × 2, two-factor design. Before the start of the formal test, the rats were randomly divided into four groups with eight replicates in each group and one rat in each replicate. All experimental procedures were approved by the Laboratory Animal Welfare and Animal Experimental Ethical Committee of the China Agricultural University (No. AW82211202–1–4). During the experiment, the indoor temperature was maintained at 24 ± 1 °C and the relative humidity was maintained at 50–60%. All rats had access to food and water during the study period.

Since previous studies found that CHP treatment for 5 days could cause significant changes in the apparent indices of rats [49], one week was chosen as the treatment period. Moreover, a COS dose of 500–600 mg/kg·BW·day can effectively induce its biological activity in rats [50, 51], and the daily intake of rats weighing approximately 200 g should be 100–120 mg/day. For example, if 200 g rats drink 22 mL of water per day, then the concentration of COS in water should be 4.55–5.45 mg/mL. Therefore, a dose of 5 mg/mL was chosen in our experiments to achieve the strongest biological activity of COS in the rats. The four groups were treated as follows: (1) CHP-/COS- group (feeding a basal diet); (2) CHP+/COS- group (feeding a basal diet + gavage administration of corn oil containing 10 mg/kg BW CHP); (3) CHP-/COS+ group (feeding a basal diet + drinking water containing 5 mg/mL COS); (4) CHP+/COS+ group (feeding a basal diet + gavage administration of corn oil containing 10 mg/kg BW CHP + drinking water containing 5 mg/mL COS).

For the first seven days, the third and fourth groups were given drinking water containing 5 mg/mL COS. For the next seven days, the third and fourth groups continued to be given drinking water containing COS, while the second and fourth groups were gavaged with 10 mg/kg BW CHP. All the rats were fed a basal diet during the study period. Nutritional levels of the basal diets are shown in Table S1.

2.2. CHP and chemicals

The CHP (# 2921–88–2) standard was purchased from Beijing Putian Tongchuang Biotechnology Co., Ltd. (Beijing, China) with a purity of 98.9%. COS (effective concentration>95%) was purchased from Qingdao Honghai Biotechnology Co., Ltd. (Qingdao, Shandong, China). The basal maintenance diet used in the experiment was purchased from Beijing Huafukang Bioscience Co., Ltd. (Beijing, China).

2.3. Preparation before gavage

Because CHP is slightly soluble in water and easily soluble in organic solvents, it was dissolved in peanut oil before gavage. CHP (20 mg) was weighed and dissolved in 10 mL of corn oil. During gavage, each rat in the CHP+/COS- and CHP+/COS+ groups was given 1.0 mL of corn oil (CHP orally administered, approximately 10 mg/kg BW) daily, and the other two groups were given the same amount of vehicle.

2.4. Sample collection

All rats were fasted overnight before slaughter and remained fasted for 12 h. Subsequently, the mice were euthanized. Blood was collected and the rat liver, spleen, and kidney organs were accurately weighed rapidly. After standing at 4 °C for 2 h, the blood was centrifuged at 3500 rpm for 15 min, and the upper serum was extracted and stored at − 80 ℃ for the determination of blood biochemical indicators.

The duodenum, jejunum, and ileum of the rats were isolated. The duodenum and jejunum without chyme were selected and placed in 4% paraformaldehyde for observation of tissue sections and immunofluorescence (IF), and another part (without chyme or without chyme after washing) was stored at − 80 °C and was used to detect other indicators. Finally, the contents of the colon and ileal tissues were collected and stored at − 80 °C for the determination of CHP residues. The isolated caecal contents were stored at − 80 °C for gut microbiota profiling via 16S rRNA amplicon sequencing.

2.5. Production performance and organ index

Each rat was weighed before starting the experiment (T1). According to the weight, the rats were injected with 1.0 mL of CHP-containing corn oil or normal corn oil. After the rats drank water containing COS for one week (T2), each rat was weighed to obtain the initial weight (IW). During this period, the daily body weight and food intake of each rat was recorded. After the experiment (T3), each rat was weighed to obtain the final weight (FW). The total feed intake of each rat in the second week was recorded, and the average daily gain (ADG) and average daily feed intake (ADFI) were calculated. The organ index was calculated from organ weights after slaughter.

2.6. Determination of CHP residues

The CHP enzyme-linked immunosorbent assay (ELISA) kit (# HB248-NC) used in this experiment was purchased from Shanghai Jinma Laboratory Equipment Co., Ltd. (Jinma, Shanghai, China). Sample pre-treatment and experimental steps were performed according to the detailed instructions of the kit.

2.7. Determination of blood biochemical indicators

The commercial kits used for the determination of blood biochemical indexes in this experiment were purchased from Nanjing Jiancheng Bioengineering Institute (Nanjing, Jiangsu, China). Measurement indicators include albumin (ALB, # A028–1–1), alkaline phosphatase (AKP, # A059–1–1), alanine aminotransferase (ALT, # C009–2–1), aspartate aminotransferase (AST, # C010–2–1), total bilirubin (TBIL, # C019–1–1), direct bilirubin (DBIL, # C019–2–1), creatinine (CRE, # C011–2–1), blood urea nitrogen (BUN, # C013–1–1) and uric acid (URIC, # C012–1–1). All assay steps were performed following the instructions in the kits.

2.8. Determination of serum neurochemical parameters

The AChE activity kit (# L–735–SH) was purchased from Shanghai Jinma Laboratory Equipment Co., Ltd. (Jinma, Shanghai, China). Acetylcholine (ACh) content kit (# A105–1–1) was purchased from Nanjing Jiancheng Bioengineering Institute (Nanjing, Jiangsu, China). All test steps were performed following the corresponding instructions in the kits.

2.9. Determination of antioxidant capacity of intestinal tissue

Commercial kits used for the determination of antioxidant indices in duodenal and jejunal tissues were purchased from Nanjing Jiancheng Bioengineering Institute (Nanjing, Jiangsu, China), including total antioxidant capacity (T-AOC, # A015–1–2), total superoxide dismutase (T-SOD, # A001–1–1), glutathione peroxidase (GPx, # A005–1–2), glutathione S-transferase (GST, # A004–1–1), catalase (CAT, # A007–1–1), hydrogen peroxide (H_2O_2, # A064–1–1), and methane dicarboxylic aldehyde (MDA, # A003–1–1). Tissue homogenates (10%) were prepared prior to testing. The sample pre-treatment steps are shown in Fig. S1. All test steps were performed according to the

manufacturer's instructions.

2.10. Observation of intestinal tissue sections

The duodenum and jejunum tissues preserved in 4% paraformaldehyde (over 24 h) were removed, and pathological tissue sections were prepared via dehydration, paraffin embedding, sectioning, dewaxing, and hematoxylin-eosin (HE) staining, and photographs were obtained using a microscope (BX63, OLYMPUS, Japan) and cellSens standard imaging software (cellSens, Japan). At least three samples were selected for observation in each group. Villus height is a measure of the vertical distance from the tip of the villi to the crypt opening. Crypt depth is the measurement of the vertical distance from the opening to the base of the crypt. Mucosal thickness is a measure of the vertical distance from the mucosal epithelium to the muscular mucosa, including the muscular mucosa.

2.11. Determination of serum inflammatory factors by enzyme-linked immunosorbent assay (ELISA)

The serum at − 80 ℃ was taken out to analyze the concentration of inflammatory factors. The ELISA kit used in the experiment was purchased from Shanghai hengyuan biological technology Co., Ltd. (Hengyuan, Shanghai, China). Measurement indicators include interleukin-1β (IL-1β, # HB1074-Mu), interleukin-6 (IL-6, # HB1061-Mu), interleukin-10 (IL-10, # HB1087-Mu), and tumour necrosis factor-α (TNF-α, # HB049-Mu). All assay steps were performed as directed by the kit.

2.12. Immunofluorescence (IF) staining

First, paraffin sections were de-paraffinized. The sections were then placed into a citrate antigen retrieval solution (# P0083, Beyotime Biotechnology, Shanghai, China) for antigen retrieval. The retrieved samples were incubated with 5% goat serum in phosphate buffered saline (PBS) for 30 min at room temperature and then stained using a fluorescently labelled primary antibody [BioLegend Biotechnology Co., Ltd. (San Diego, CA, US)] against inflammatory cell markers (CD11b, # 101207; CD64, # 139316; F4/80, # 123108; CD3, # 100204; CD19, # 115507). The jejunal sections were additionally incubated using a primary antibody against tight junction proteins without fluorescent labelling, which was purchased from Sangon Biotech (Shanghai) Co., Ltd. (Claudin-1, # D260403) and Proteintech Co., Ltd. (USA) [Zona occludin-1 (ZO-1), # D264329; Occludin, # 13409–1-AP]. The sections were then incubated using a secondary antibody (# HX2074, Beijing Huaxingbio Genetic Technology Co., Ltd.) from the same source as the primary antibody with fluorescent labelling. Nuclei were counterstained using 4',6-diamidino-2-phenylindole (DAPI) (# C0065, Beijing Solarbio Science & Technology Co., Ltd. Beijing, China) and then rinsed using PBS to remove the excess staining solution. Finally, the slides were mounted using an anti-fluorescence decay mounting medium (# S2100, Beijing Solarbio Science & Technology Co., Ltd. Beijing, China) and observed using laser scanning confocal microscopy (LSCM) (ECLIPSE Ti2, Nikon, Japan). An imaging software analysis platform (Nikon NIS-Elements AR, Nikon, Japan) was used for imaging.

2.13. Detection of apoptosis by terminal deoxynucleotidyl transferase-mediated dUTP nick-end labelling (TUNEL) method

The experimental operation was performed according to the instructions of the one-step TUNEL apoptosis assay kit (# C1086) produced by Beyotime Biotechnology Co., Ltd. (Shanghai, China). Nuclei were stained with DAPI (# G8170, Beijing Solarbio Science & Technology Co., Ltd. Beijing, China) and immediately photographed with an LSCM (ECLIPSE Ti2, Nikon, Japan). Finally, the image software analysis platform (Nikon NIS-Elements AR, Nikon, Japan) was used for imaging.

2.14. Quantitative real-time polymerase chain reaction (qRT-PCR)

First, total RNA from the intestinal tissue was extracted using TRIZON. The concentration of total RNA was determined using a Nano Photomeyer P-Class (Implen GmbH, Munich, Germany). RNA (4000 ng) was reverse-transcribed into 10 μL of cDNA using a reverse transcription kit Yeasen Biotechnology Co., Ltd., Shanghai, China, # 11120ES60). The reverse transcription system (10 μL) included (1) 5 μL of 2 × HifairR II Super Mix and (2) 5 μL of template RNA+ddH_2O. The specific operation steps were performed according to the manufacturer's instructions.

The reverse-transcribed cDNA was diluted 16-fold for qRT-PCR (ABI 7500, Alameda, CA, USA). A qRT-PCR kit (# PC6002) was purchased from Beijing Aidlab Biotechnologies Co., Ltd. (Beijing, China). The total reaction volume was 10 μL, including (1) 5 μL of 2 × SYBR qPCR Mix (Low ROX), (2) 1 μL of DNA Template, (3) 0.2 μL of Forward Primer (10 Mm), (4) 0.2 μL of Reverse Primer (10 μM), and (5) 3.6 μL of ddH_2O. The primer sequences used are listed in Table S2 (Supplementary Material). The reaction was run for one cycle at 95 °C for 2 min, 40 cycles at 95 °C for 15 s, and 60 °C for 34 s. The results were calculated and analysed using the $2^{-\Delta\Delta Ct}$ method, based on the final output Ct value of the housekeeping gene glyceraldehyde-3-phosphate dehydrogenase (GAPDH) and the target gene.

2.15. Western blot analysis

The jejunum samples stored at − 80 °C were fully ground in liquid nitrogen to extract tissue proteins, and the protein concentration of the samples was determined using the bicinchoninic acid method. The final protein loading was 40 ng, according to the protein concentration. Sodium dodecyl sulphate-polyacrylamide gel electrophoresis (10%) was used to separate protein molecules of different molecular weights, which were then transferred to a polyvinylidene fluoride (PVDF) (Beyotime Biotechnology, Shanghai, China) membrane with a 0.45-μm pore size. After removing the PVDF membrane, it was blocked using 5% bovine albumin for 2 h. According to the instructions of the protein marker, the target molecule bands were then cut out and incubated overnight with the corresponding primary antibodies at 4 °C. After washing the PVDF membrane the next day, it was incubated with an HRP-labelled secondary antibody for 2 h at room temperature and photographed using the Image Quant LAS 4000 mini system (GE Healthcare, Piscataway, NJ, USA) after washing. All primary and secondary antibodies were diluted in accordance with the manufacturer's instructions. As a reference, the grey value of each target protein was compared with that of β-actin to obtain the relative expression of the protein.

2.16. Metabolomics profiling

Metabolite detection was provided by Wekemo Tech Group Co., Ltd. Shenzhen China. The data were analyzed on the free online platform of Wekemo Bioincloud. The figures in the results were completed using the Wekemo Bioincloud (https://www.bioincloud.tech). The metabolites extraction, UHPLC-MS/MS analysis, data processing, and metabolite identification involved in the experimental process are shown in Supplementary Material.

2.17. Gut microbiota profiling by 16S rRNA amplicon sequencing

Sequencing service was provided by Wekemo Tech Group Co., Ltd. Shenzhen China. The data were analyzed on the free online platform of Wekemo Bioincloud. The figures in the results were completed using the Wekemo Bioincloud (https://www.bioincloud.tech). The DNA extraction and PCR amplification, Illumina Novaseq sequencing, and information analysis involved in the experimental process are shown in Supplementary Material.

2.18. Statistical analyses

The data analysis software SPSS 16.0 (IBM-SPSS Inc., Chicago, IL, USA) was used to process and analyse the experimental data using analysis of variance (ANOVA) with a 2 × 2 factorial arrangement. The statistics calculated included the effects of CHP and COS on the rats and their interactions. Differences among groups were evaluated using one-way ANOVA and Tukey's post-hoc test. $P < 0.05$ was considered statistically significant. All figures were prepared using Adobe Photoshop (Adobe Photoshop CS5, Inc., San Jose, California, USA), GraphPad Prism

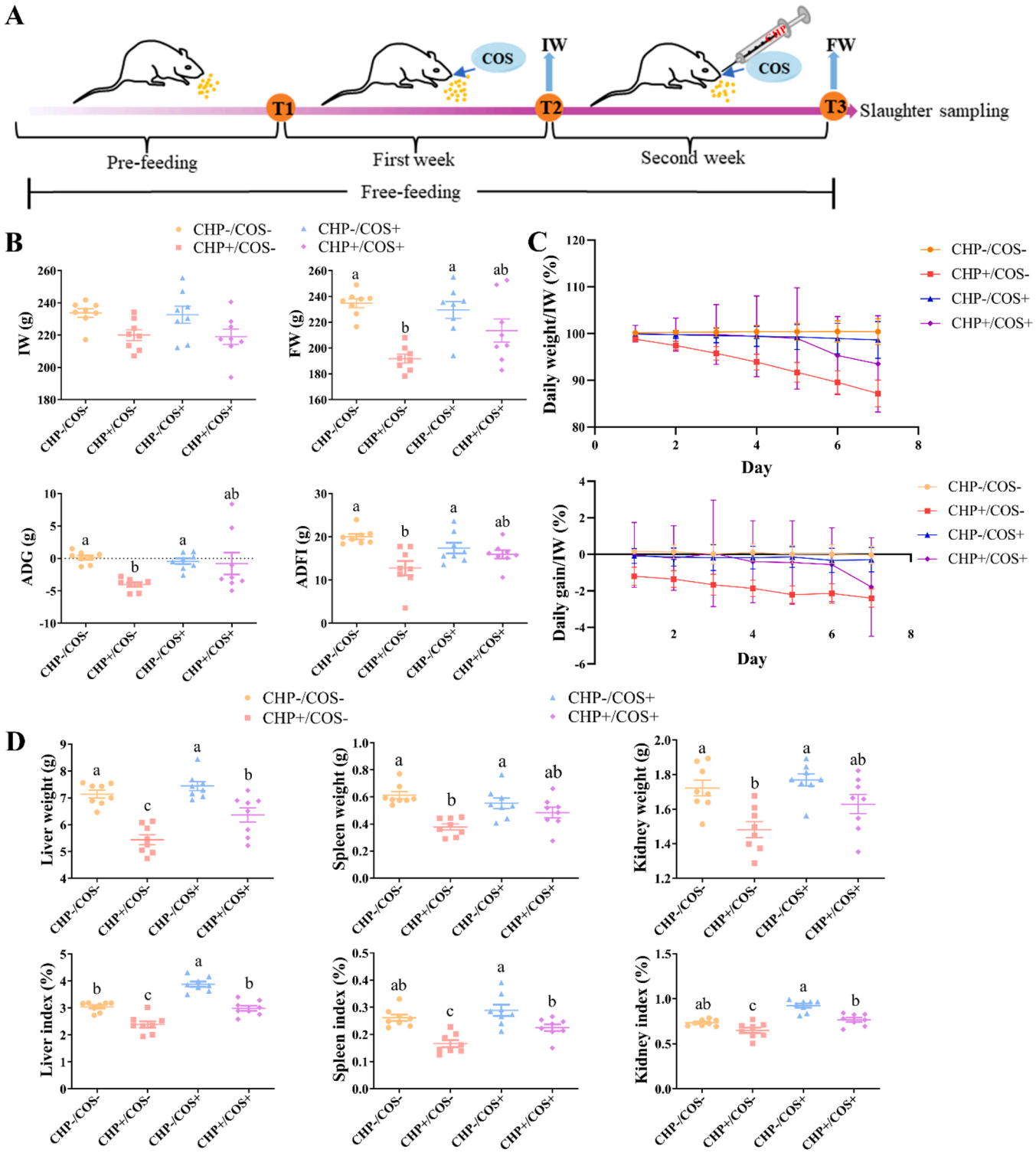

Fig. 1. (A) Experimental period and processing time; (B-C) COS alleviates the effects of CHP-induced production performance and the curves of daily weight and daily gain to initial weight ratio over time; (D) COS alleviates the effects of CHP-induced organ weight and the organ index in rats. COS-, drinking normal water; COS+, drinking water containing 5 mg/mL COS; CHP-, gavage corn oil; CHP+, gavage administration corn oil containing 10 mg/kg BW CHP. [a,b,c] For each parameter, different lowercase letters represent significant differences at $P < 0.05$. Values are the means from 8 individual rats and are presented as the mean ± SEM. CHP, Chlorpyrifos; COS, Chitosan oligosaccharide; IW, Initial weight; FW, Final weight; ADG, Average daily gain; ADFI, Average daily feed intake.

(version 5.0, Graph Pad Software Inc., San Diego, CA, USA), and PowerPoint in Microsoft 365. The correlation analysis between the gut microbiome and metabolites was investigated using the Spearman correlation test by R 4.2.2. $P < 0.05$ was considered significant.

3. Results

3.1. Growth performance and organ index

A schematic diagram of each treatment programme is shown in Fig. 1A. The daily body weight and food intake of the rats were recorded during the experiment to calculate the production performance. The results revealed a significant decrease in FW, ADFI, and ADG in the CHP-

A CHP residues in the ileum and colonic contents of rats in different treatments

Items	COS-		COS+		SEM	*P*-value		
	CHP-	CHP+	CHP-	CHP+		CHP	COS	CHP×COS
Ileum (ppb)	0.250^{b}	0.373^{a}	0.213^{b}	0.259^{b}	0.013	<0.001	<0.001	0.015
Colonic contents (ppb)	0.194^{c}	0.243^{b}	0.197^{c}	0.271^{a}	0.007	<0.001	0.018	0.045
Ileum/colon contents	1.299^{ab}	1.546^{a}	1.087^{bc}	0.964^{c}	0.054	0.424	<0.001	0.022

^{a,b,c} For each parameter, the values with different small superscript letters indicate a significant difference (P<0.05).

B

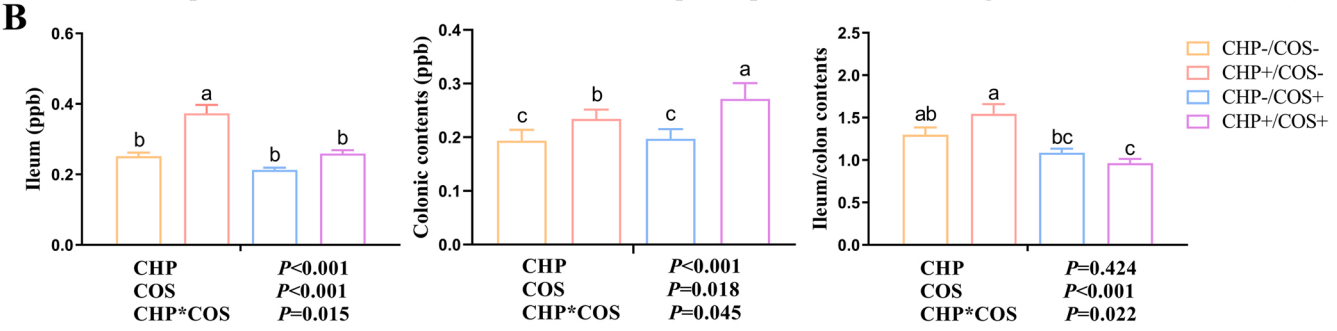

C COS alleviates the effect of CHP on the blood biochemical level in rats

Items	COS-		COS+		SEM	*P*-value		
	CHP-	CHP+	CHP-	CHP+		CHP	COS	CHP×COS
ALB (g/L)	36.12	37.46	37.48	34.64	0.623	0.553	0.559	0.104
AKP (U/L)	116.29	111.24	91.67	135.80	9.440	0.314	0.999	0.207
ALT (U/L)	28.24	27.65	23.88	23.38	0.963	0.771	0.028	0.979
AST (U/L)	21.59^{b}	33.55^{a}	25.31^{b}	27.40^{ab}	1.164	0.001	0.500	0.010
AST/ALT	0.77^{b}	1.26^{a}	1.11^{ab}	1.19^{a}	0.058	0.008	0.168	0.051
TBIL (μmol/L)	2.35	2.45	2.47	2.70	0.094	0.402	0.356	0.750
DBIL (μmol/L)	0.79	1.00	0.87	0.66	0.058	0.983	0.260	0.076
CRE (μmol/L)	49.84	43.36	41.83	43.16	1.280	0.296	0.101	0.118
BUN (mmol/L)	3.83	3.99	4.74	5.04	0.210	0.568	0.020	0.866
URIC (mg/L)	48.66	49.30	49.76	49.06	0.318	0.969	0.513	0.314

^{a,b} For each parameter, the values with different small superscript letters indicate a significant difference (P<0.05).

D

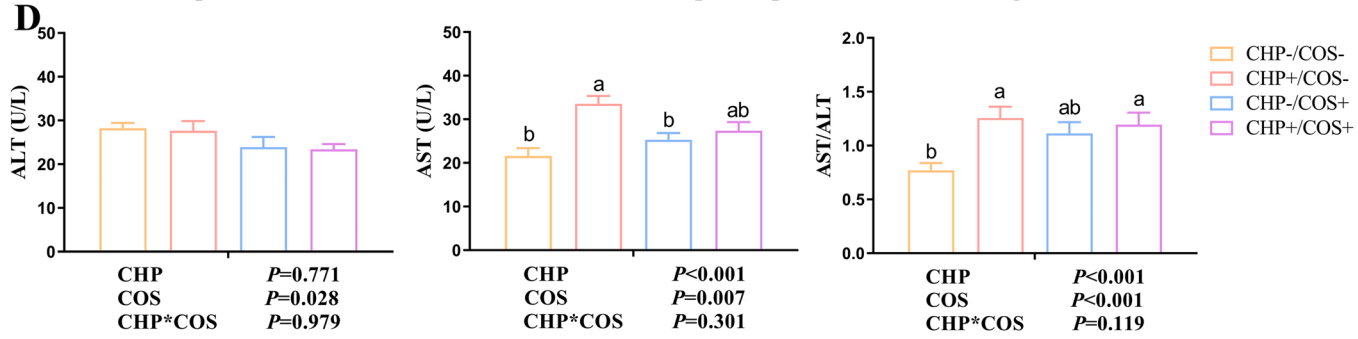

Fig. 2. Residual status of CHP and COS alleviates the effect of CHP on the blood biochemical level in rats. (A-B) Residual levels of CHP in ileal and colonic contents and the proportion of ileal/colonic contents on rats in different treatment groups; (C-D) Alleviating effect of COS on CHP-induced abnormal blood biochemical levels in rats. ^{a,b,c} For each parameter, different lowercase letters represent significant differences at $P < 0.05$. SEM: pooled standard error of the means. Values are the means from 8 individual rats and are presented as the mean ± SEM. The P values represent the main effect of COS, the main effect of CHP, or the interaction of COS and CHP. The annotation of CHP and COS can be seen in the legend of Fig. 1.

treated group compared with the control group ($P < 0.05$). FW, ADG, and ADFI were significantly higher in the CHP+/COS+ group than in the CHP-treated group ($P < 0.05$), and there was no significant difference between the CHP+/COS+ and control groups (Fig. 1B). In addition, to show the daily trend of body weight and daily weight gain of the rats, the curves in Fig. 1C were obtained by calculating the ratio of the two to IWs. The ratio of daily body weight and daily weight gain to IW in the CHP-treated group exhibited a decreasing trend over time. At the end of the experiment, the weight of each organ was measured, and it was found that the weights of the liver, spleen, and leftover and their respective organ indices were significantly decreased in the CHP-treated rats compared with the control group ($P < 0.05$), while the COS remission group (CHP+/COS+) showed a significant increase compared to the CHP-treated group ($P < 0.05$) (Fig. 1D). This suggests that exposure to CHP can reduce the productive performance of rats and that COS can resist this effect induced by CHP.

3.2. Residues of CHP in ileal and colonic contents

To determine the absorption of CHP in vivo, the residual amount of CHP in the ileal and colonic contents of rats was measured, and the ratio of CHP in the ileal and colonic contents was calculated (Fig. 2A-B). It can be seen from the results that, after the rats were protected by COS (CHP+/COS+ group), the content of CHP in the ileum tissue was significantly lower than that in the CHP+/COS- group ($P < 0.05$), but the content of CHP in the colonic content was significantly higher than that in the CHP+/COS- group ($P < 0.05$). Moreover, based on the proportion of CHP residues between the ileum and colon contents, the amount of CHP absorbed by the body was normally greater than the amount excreted (ratio > 1). After COS protection, absorption in the body decreased and excretion increased (ratio < 1). This indicates that COS can effectively inhibit CHP absorption.

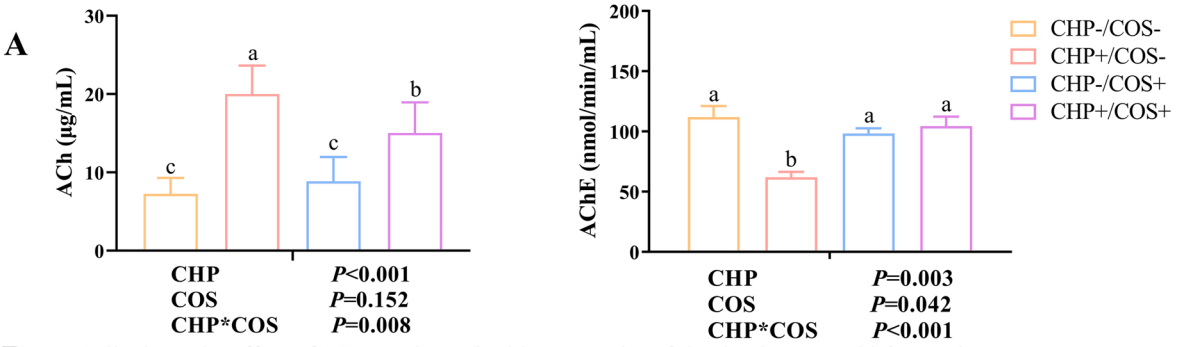

B COS alleviates the effect of CHP on the antioxidant capacity of the duodenum and jejunum in rats

Items	COS-		COS+		SEM	*P*-value		
	CHP-	CHP+	CHP-	CHP+		CHP	COS	CHP×COS
Duodenum								
T-AOC (U/mg prot)	2.08	2.03	1.99	1.91	0.039	0.452	0.210	0.864
T-SOD (U/mg prot)	22.54	25.18	24.40	22.00	0.600	0.919	0.577	0.039
GPx (U/mg prot)	21.96	22.03	21.58	21.44	0.580	0.975	0.692	0.936
GST (U/mg prot)	232.81	219.25	217.08	226.06	3.766	0.765	0.561	0.148
CAT (U/mg prot)	55.01^{b}	51.75^{b}	93.41^{a}	54.92^{b}	3.885	<0.001	<0.001	0.001
H_2O_2 (mg/g prot)	22.03	26.23	24.36	23.96	0.630	0.125	0.982	0.066
MDA (nmol/mg prot)	1.05	1.27	1.03	1.09	0.041	0.082	0.214	0.293
Jejunum								
T-AOC (U/mg prot)	3.14	3.04	2.96	2.98	0.074	0.812	0.430	0.692
T-SOD (U/mg prot)	29.30	22.53	26.00	22.54	1.128	0.023	0.445	0.443
GPx (U/mg prot)	58.82	42.30	49.10	42.29	2.550	0.020	0.311	0.313
GST (U/mg prot)	212.30	193.78	223.65	195.57	4.821	0.015	0.472	0.600
CAT (U/mg prot)	62.54^{c}	84.67^{bc}	102.28^{ab}	110.92^{a}	4.432	0.019	<0.001	0.283
H_2O_2 (mg/g prot)	20.39	23.09	21.55	21.72	0.679	0.307	0.937	0.367
MDA (nmol/mg prot)	1.09	1.36	1.08	1.20	0.036	0.005	0.198	0.287

[a, b, c] For each parameter, the values with different small superscript letters indicate a significant difference ($P<0.05$).

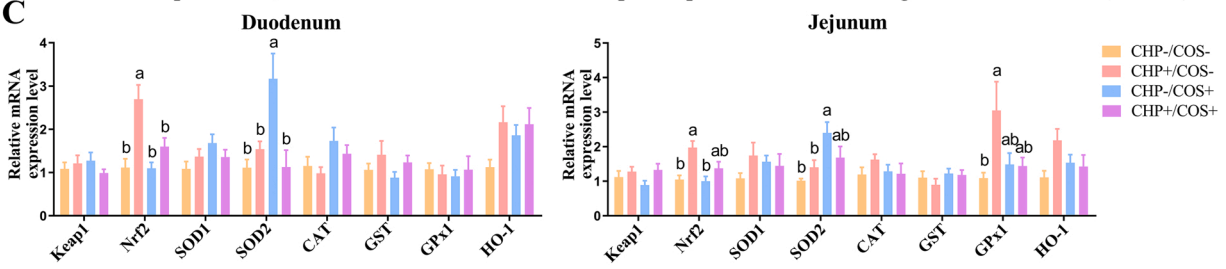

Fig. 3. COS alleviates CHP-induced neurotoxicity and changes antioxidant capacity in rats. (A) COS alleviates CHP-induced changes in serum ACh content and AChE activity in rats; (B) Determination of antioxidant capacity in rats' duodenum and jejunum tissues; (C) Expression of genes related to the Keap1/Nrf2 signalling pathway in rats. The annotation of CHP, COS, SEM, *P* values, and [a,b,c] can be seen in the legend of Fig. 2.

3.3. Effect of CHP, COS, and combined effects on blood biochemical parameters

To evaluate the effect of CHP on liver and kidney function in rats and the protective effect of COS, we measured the blood biochemical levels of the experimental rats in each group, and the results are shown in Fig. 2C-D. As shown in the figure, oral CHP at a concentration of 10 mg/kg BW had no significant effect on ALB, ALP, ALT, TBIL, DBIL, CRE, BUN, or URIC levels in the rats ($P > 0.05$). However, oral CHP significantly affected the AST index ($P < 0.05$), which significantly decreased with oral COS dose ($P < 0.05$). This suggests that CHP can induce abnormal liver function in rats and that COS can effectively protect liver function.

3.4. Neurochemical parameters in serum

Reduced AChE activity is one of the most significant manifestations of OPP poisoning. The measured neural parameters included AChE

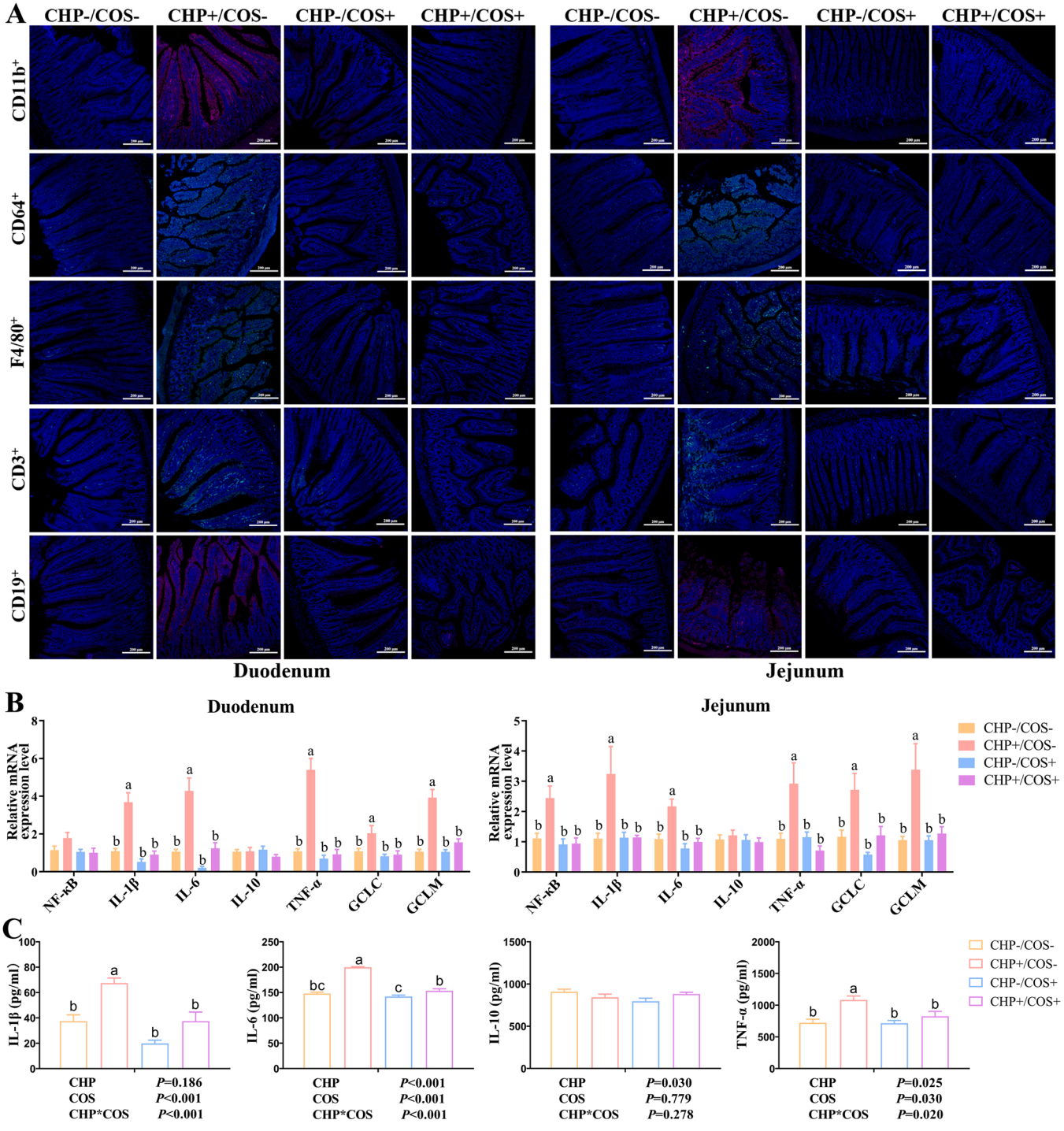

Fig. 4. COS attenuates CHP-induced inflammatory cell infiltration and expression of inflammatory cytokines in rats. (A) Inflammatory cells markers in the duodenum and jejunum of rats in different treatment groups was determined by IF; (B) Expression of related genes of inflammatory factors in the duodenum and jejunum of rats in different treatment groups; (C) Levels of inflammatory factors in the serum of rats in different treatment groups. The annotation of CHP, COS, SEM, *P* values, and ^{a,b,c} can be seen in the legend of Fig. 2.

activity and ACh content (Fig. 3A). AChE activity was significantly inhibited at a CHP dose of 10 mg/kg BW compared with that in the control group ($P < 0.05$). There was a significant increase in AChE activity after COS treatment ($P < 0.05$). Since the substrate of AChE is the neurotransmitter ACh, reduced AChE activity leads to excessive accumulation of ACh in target organs and causes neurological dysfunction. Although COS protection resulted in a decreasing trend in ACh content with increasing AChE activity, it could not be restored to the same level as the control group.

3.5. COS attenuates CHP-induced changes in intestinal anti-oxidation

To understand the effect of CHP on intestinal antioxidant levels in rats and the intervention effect of COS, the levels of antioxidant-related indicators in the duodenal and jejunal tissues were measured, as shown in Fig. 3B. It can be seen that COS could significantly enhance the activity of CAT in tissues ($P < 0.05$) and showed a significant alleviation effect on CHP-treated rats ($P < 0.05$).

Therefore, to further verify the alleviating effect of COS on CHP-induced changes in antioxidant capacity at the molecular level, we measured the relative mRNA expression of genes in the Keap1/Nrf2

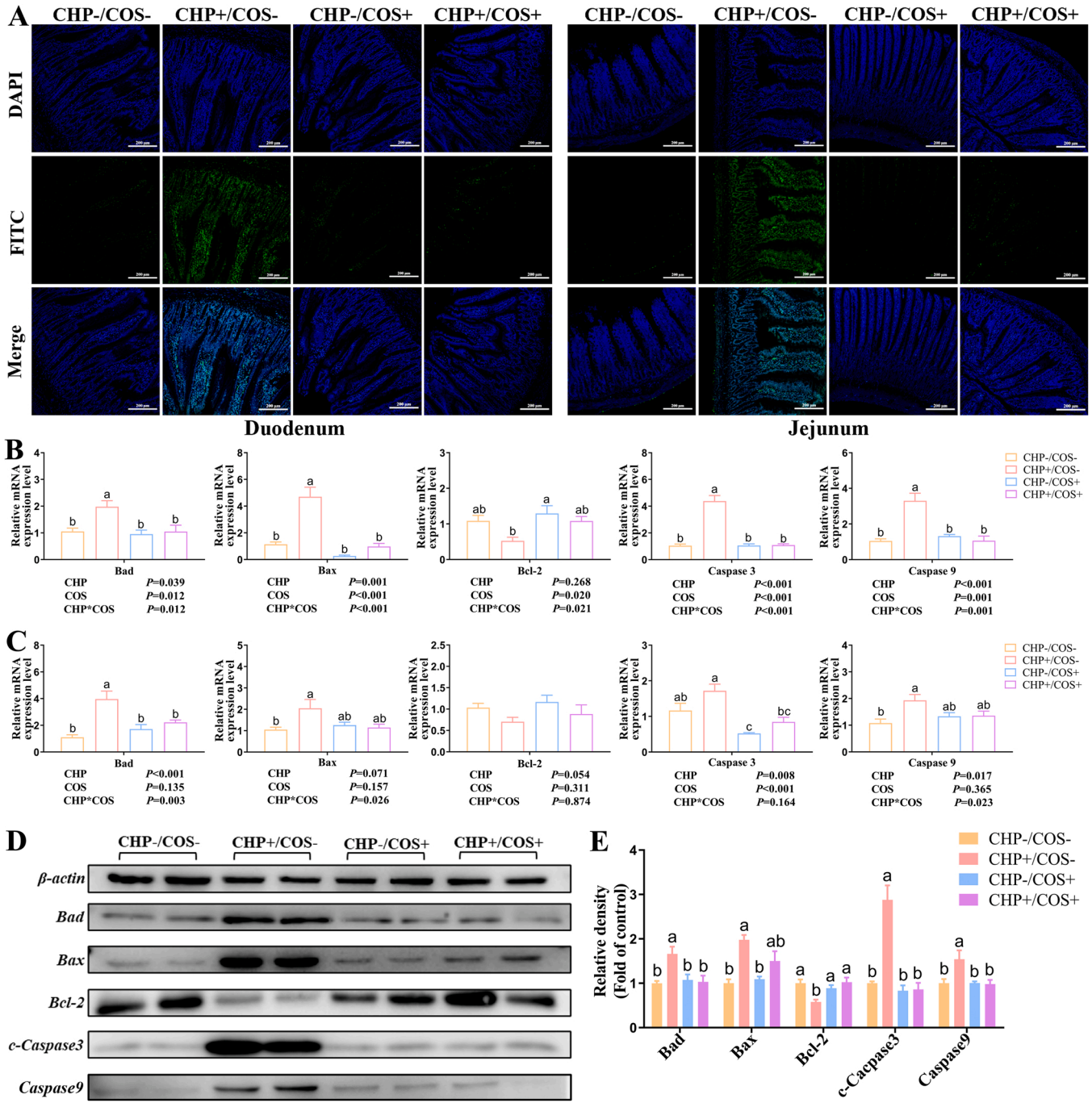

Fig. 5. COS attenuates CHP-induced apoptosis in intestinal cells. (A) Apoptosis of duodenum and jejunum of rats in different treatment groups was measured using the TUNEL method; (B-C) Relative gene expression of pro-apoptotic and anti-apoptotic factors in NF-κB signalling pathway in the duodenum and jejunum of rats in different treatment groups; (D-E) Protein expression of pro-apoptotic and anti-apoptotic factors in NF-κB signalling pathway in jejunum of rats of different treatment groups. The annotation of CHP, COS, SEM, *P* values, and [a,b] can be seen in the legend of Fig. 2.

antioxidant signalling pathway in the jejunum and duodenum (Fig. 3C). The results showed that oral CHP significantly increased the expression of the nuclear factor erythroid 2-related factor 2 (Nrf2) gene in the duodenum and jejunum ($P < 0.05$). When measuring the relative expression of downstream genes of this pathway, we found that the relative expression of the superoxide dismutase in mitochondrial (SOD2) gene in the oral COS group (CHP-/COS+) was significantly higher than that in the control group ($P < 0.05$), indicating that COS stimulates organismal antioxidant defence. In the jejunum, we also found that oral administration of CHP caused a significant upregulation of glutathione peroxidase cytoplasm (GPx1) gene expression in tissues ($P < 0.05$), while it was significantly downregulated after oral administration of COS ($P < 0.05$). This suggests that the organism may resist CHP-induced oxidative damage by activating its own GPx1 activity in the absence of active substance intervention.

3.6. COS attenuates CHP-induced intestinal inflammation in rats

First, we analysed the number of inflammatory cells in the duodenum and jejunum of the rats in each group using IF. As shown in Fig. 4A, COS significantly reduced the increase in inflammatory cells ($CD11b^+$, $CD64^+$, $F4/80^+$, $CD3^+$, and $CD19^+$) induced by CHP in the duodenum and jejunum ($P < 0.05$), indicating that COS can effectively alleviate the inflammatory effect of the small intestine. In addition, in the determination of relative mRNA expression and protein expression in jejunum and duodenum (Fig. 4B-C), COS could effectively alleviate the high expression of pro-inflammatory factors (IL-1β, IL-6, and TNF-α) and the high expression of chemokines [glutamate cysteine ligase catalyses subunit (GCLC) and glutamic acid cysteine ligase modified subunit (GCLM)] in mRNA expression caused by CHP ($P < 0.05$). Moreover, COS significantly reversed the high mRNA expression of nuclear factor kappa B (NF-κB) induced by CHP ($P < 0.05$). This indicates that COS can effectively control CHP-induced inflammatory responses in rats at the molecular level.

3.7. COS attenuates CHP-induced apoptosis in intestinal cells

To further prove the protective effect of COS on the intestinal barrier, we used the TUNEL assay to detect apoptosis in the duodenum and jejunum of the rats. As shown in Fig. 5A, the number of apoptotic cells (green fluorescence) in the duodenum and jejunum of rats triggered by CHP treatment (CHP+/COS- group) was higher than that in the control group. The number of apoptotic cells was significantly reduced in the tissues of rats cotreated with COS and CHP (CHP+/COS+ group).

At the molecular level, we examined gene and protein expression associated with the nuclear factor kappa B (NF-κB) apoptosis signalling pathway in further. COS can effectively suppress the upregulation of pro-apoptotic genes [Bcl2 associated death promoter (Bad), Bcl2-associated X (Bax), caspase-3, and caspase-9] and alleviate the downregulation of anti-apoptotic genes [B-cell lymphoma-2 (Bcl-2)] in the duodenum and jejunum caused by CHP (Fig. 5B-C). Moreover, COS significantly inhibited the upregulation of pro-apoptotic proteins and promoted the expression of anti-apoptotic proteins in the jejunum induced by CHP at the protein level ($P < 0.05$) (Fig. 5D-E). This indicates that COS has a good inhibitory effect on CHP-induced excessive apoptosis in rat intestinal cells, which is beneficial for maintaining intestinal homoeostasis.

3.8. COS attenuates CHP-induced intestinal barrier damage in rats

Intestinal villi morphology can effectively respond to the integrity of the intestinal barrier. Therefore, we performed HE staining of the duodenum and jejunum to determine the effect of CHP on intestinal barrier damage and COS. The results showed that the intestinal villi of the CHP-treated group (CHP+/COS-) were sparsely arranged and the tips of the villi were slightly damaged. After COS protection (CHP+/COS+), the morphology of the intestinal villi significantly improved, showing a dense and regular arrangement (Fig. 6A). After measurement and calculation, we found that oral administration of COS in the rats significantly inhibited CHP-induced reduction in villus height (jejunum) and crypt depth increase (duodenum) and balanced the villi to crypt ratio (V/C) ($P < 0.05$) (Fig. 6B). This suggests that COS plays a positive role in protecting against CHP-induced changes in the intestinal morphology.

In addition, we measured the gene and protein expression of tight junction proteins ZO-1, Claudin-1, and Occludin (Fig. 6C-D). It can be seen from the figure that COS can effectively alleviate the decrease in ZO-1, Claudin-1, and Occludin expression in the duodenum and jejunum caused by CHP when co-treated with CHP ($P < 0.05$). In detecting the localisation of tight junction proteins (Fig. S2) in the jejunum, we also found results consistent with gene and protein expression. This suggests that COS can effectively protect the integrity of the intestinal barrier from damage by CHP at the molecular level.

3.9. Metabolite alterations in rats in different treatment groups

Metabolomics is a research method used to determine the relative relationships between metabolites and physiological and pathological changes. Therefore, we used LC-MS/MS-based metabolomics to determine the intestinal metabolome. Among them, the grouped percentage stacking histogram and grouped clustering heat map can visualise the proportion of different metabolites in the intestine (Fig. 7A-B). The results showed that oleamide accounted for the largest proportion of the metabolites in each group. Metabolites oleamide, oleoyl ethylamide, fenpropimorph, L-(-)-methionine, L-tyrosine, indole-3-acrylic acid, and DL-Tryptophan in the CHP+/COS- group had the greatest differences with other experimental groups, and there was no significant difference between the CHP+/COS+ group and the control group. Principal component analysis (PCA) was performed to observe the metabolic differences between the control and CHP+/COS- groups. The PCA plot (Fig. 7C) showed that the samples from the CHP+/COS- group and the other groups were distributed in different areas, indicating that the cardiometabolic groups were significantly different than the CHP+/COS- group. To eliminate and highlight the differences between the groups, we performed partial least-squares discriminant analysis (PLS-DA) to analyse the samples of each group. As shown in Fig. 7D, significant differences were found between the CHP-treated, CHP-/COS+, and CHP+/COS+ groups, whereas the PCA results for the CHP-/COS+ and CHP+/COS+ groups were highly similar. In addition, from the results of random forest and support vector machine analysis, it was verified that the accuracy of the sample grouping prediction in this experiment satisfied the reliability of the data model (Fig. S3A-B). These results indicate that COS is an effective protective agent against CHP-induced jejunal metabolic abnormalities.

Based on this, we used the t-test to calculate *P*-values and fold changes to plot volcano plots. Based on the annotated results in the corresponding databases, we finalised the differential metabolites between groups ($P < 0.05$). Differential metabolites in the CHP+ /COS-, CHP-/COS+ , and CHP+ /COS+ groups compared to the controls included nucleotide metabolism (S7p), amino acid metabolism (Urocanic acid, Phenylpyruvic acid), protein metabolism (ANH, Methyl Violet), antibiotic biosynthesis (Kanosamine, ACar 18:3, ACar 14:2), lipid metabolism (4-Butylresorcinol, Estriol, Sebacic acid, lysoPA 16:0, Chenodeoxycholic Acid, Etiocholanolone), and carbohydrate metabolism (Solanine, YLX) (Fig. S3C-E). Only one metabolite was significantly downregulated in the CHP+/COS+ group compared to the CHP-/COS+ group, but 13 were significantly upregulated (Fig. S3F). At the same time, the 25 features with the most significant differences between the groups were selected, and a boxplot was drawn using ANOVA to show the data dispersion (Fig. S4). (For an explanation of the colours in this legend, the reader is referred to the web version of this article).

In addition, a t-test (or ANOVA) was used to identify significantly

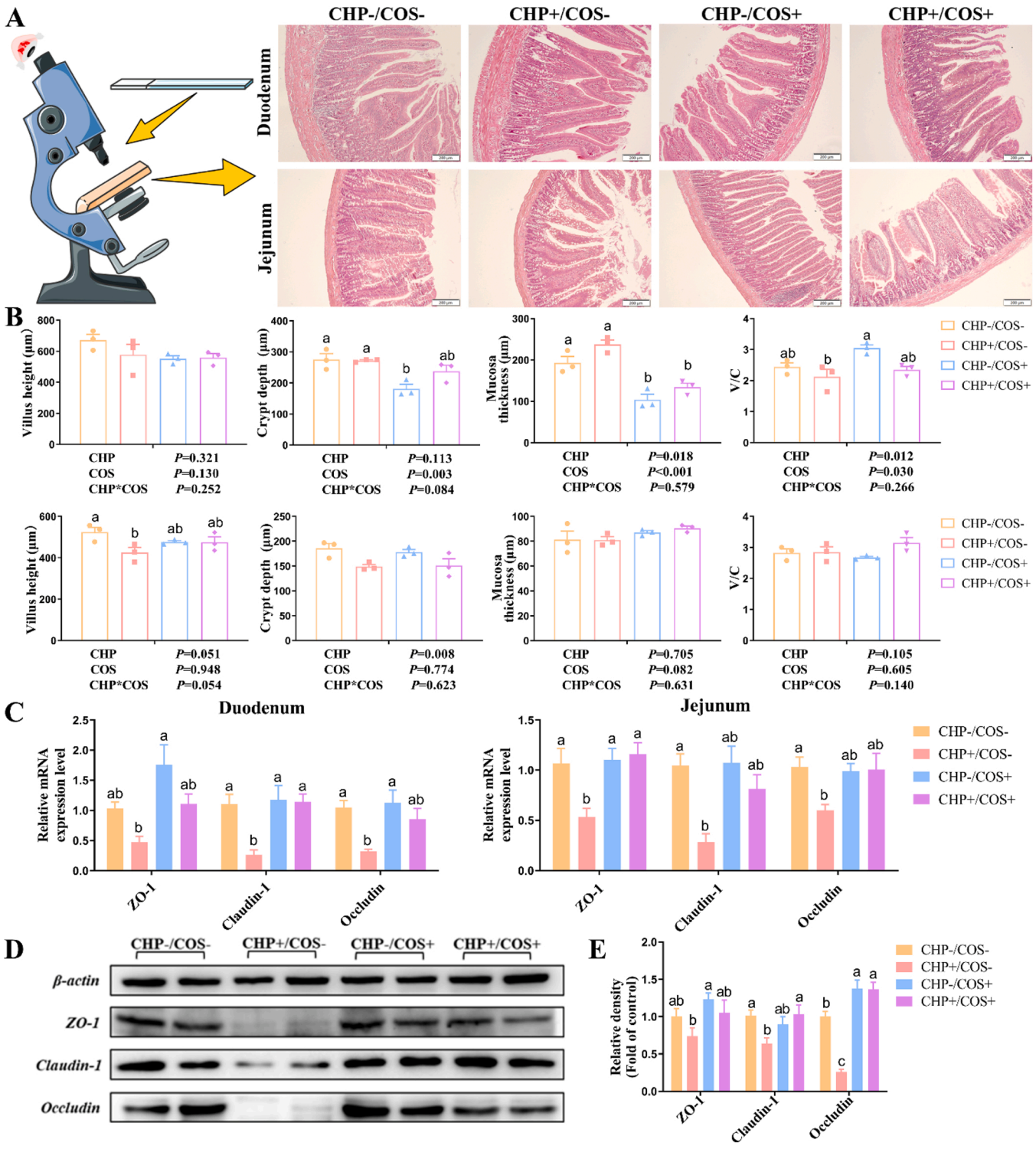

Fig. 6. COS attenuates CHP-induced intestinal barrier damage in rats. (A) HE staining of duodenum and jejunum of rats in different treatment groups; (B) Villus height, crypt depth, mucosal thickness, and villi to crypt ratio in duodenum and jejunum of rats in different treatment groups; (C) Expression of tight junction proteins in the duodenum and jejunum of rats in different treatment groups; (D-E) Protein expression of rat jejunal tight junction proteins in different treatment groups. The annotation of CHP, COS, SEM, *P* values, and [a,b,c] can be seen in the legend of Fig. 2.

different metabolites, over-representation analysis was used to find the Kyoto Encyclopedia of Genes and Genomes (KEGG) pathways that were significantly enriched by these metabolites, and the topological influence was calculated. To elucidate specific pathways, the -log10 (P) threshold was set to 1.301 to filter the pathways annotated through the KEGG database. The 44 important metabolic pathways were specifically annotated (Fig. 8A). The bubble plot shows the top 20 pathways that were significantly enriched in KEGG (Fig. 8B). The size of the bubbles indicates the degree of enrichment of the metabolic pathways involved. The three most significantly enriched pathways shown in the figure are phenylalanine, tyrosine, and tryptophan biosynthesis (Fig. 8C), D-glutamine and D-glutamate metabolism (Fig. S5A), and histidine metabolism (Fig. S5B), respectively. This indicates that COS can effectively relieve and remove metabolic disorders caused by CHP by regulating

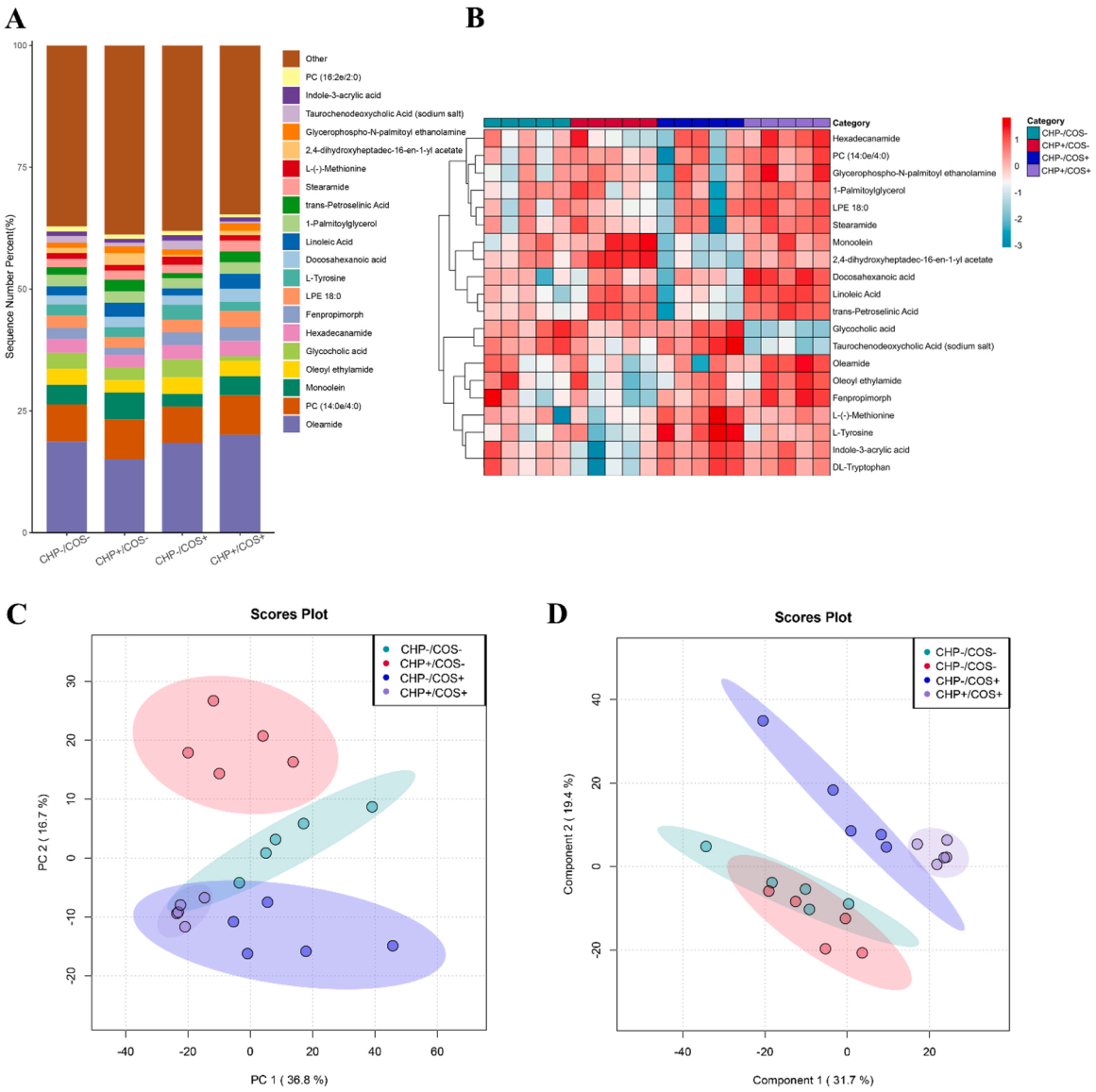

Fig. 7. Changes in jejunal metabolites in rats of different treatment groups. (A) The 10 most dominant metabolites across different treatment groups are plotted; (B) Heatmap obtained using clustering analysis of the top 20 ANOVA test metabolites in rat jejunum of different treatment groups; (C) Differences in the first two principal components of jejunal metabolites in the rat jejunum of different treatment groups were plotted on the x-axis and y-axis using principal component analysis (PCA); (D) Partial least-squares discriminant analysis (PLS-DA) score plot derived from normalised data of rat jejunum in different treatment groups. The annotation of CHP and COS can be seen in the legend of Fig. 1; n = 5 per group.

amino acid metabolism in the jejunum tissue.

3.10. COS regulated the rat gut microbiota composition of CHP-induced alterations

Gut microbiota plays a key role in regulating the intestinal barrier. Therefore, it is necessary to study the composition of CHP-induced intestinal flora in rats. The gut microbiota of rat caecal contents was analysed using 16S rRNA amplicon sequencing. As shown in Fig. 9A, the CHP-treated groups (CHP+/COS-, CHP+/COS+) showed a significant decrease in the relative abundance of *Lactobacillus* at the genus level ($P < 0.05$) compared with the CHP-/COS- group. The Venn diagram showed the number of unique bacterial operational taxonomic units (OTUs) in the gut microbiota of rats in different treatment groups (Fig. 9B), which can also reflect the diversity of the intestinal microbiome. The results showed that the four treatment groups shared 591 OTUs. Moreover, the number of unique OTUs in the CHP-treated groups was significantly reduced compared to that in the control group (CHP-/COS-) ($P < 0.05$). However, COS had no significant effect on CHP-induced changes in microbial composition or the number of bacterial OTUs. Moreover, Chao1, OTUs, Faith's phylogenetic diversity, and the Shannon index in alpha diversity reflected changes in the diversity and richness of the gut microbiota in the different treatment groups (Fig. 9C). It was found that the combined use of CHP significantly reduced the Chao1 and OTUs indices ($P < 0.05$) but had no significant effect on the Shannon and Faith's phylogenetic diversity indices. The combination of CHP and COS did not affect the Chao1 and OTU indices. Bray–Curtis dissimilarity and weighted UniFrac distance results were obtained using non-metric multidimensional scaling (NMDS) analysis (Fig. 9D). This is a measure of beta diversity in the distribution of the faecal microbiome across treatments and a measure of similarity in microbial composition between individuals. The results showed no significant differences among the different treatment groups. Additionally, principal coordinate analysis (PCoA) based on these two methods can assess structural changes in the gut microbiota to better assess the heterogeneity of beta diversity. The results showed that the microbial

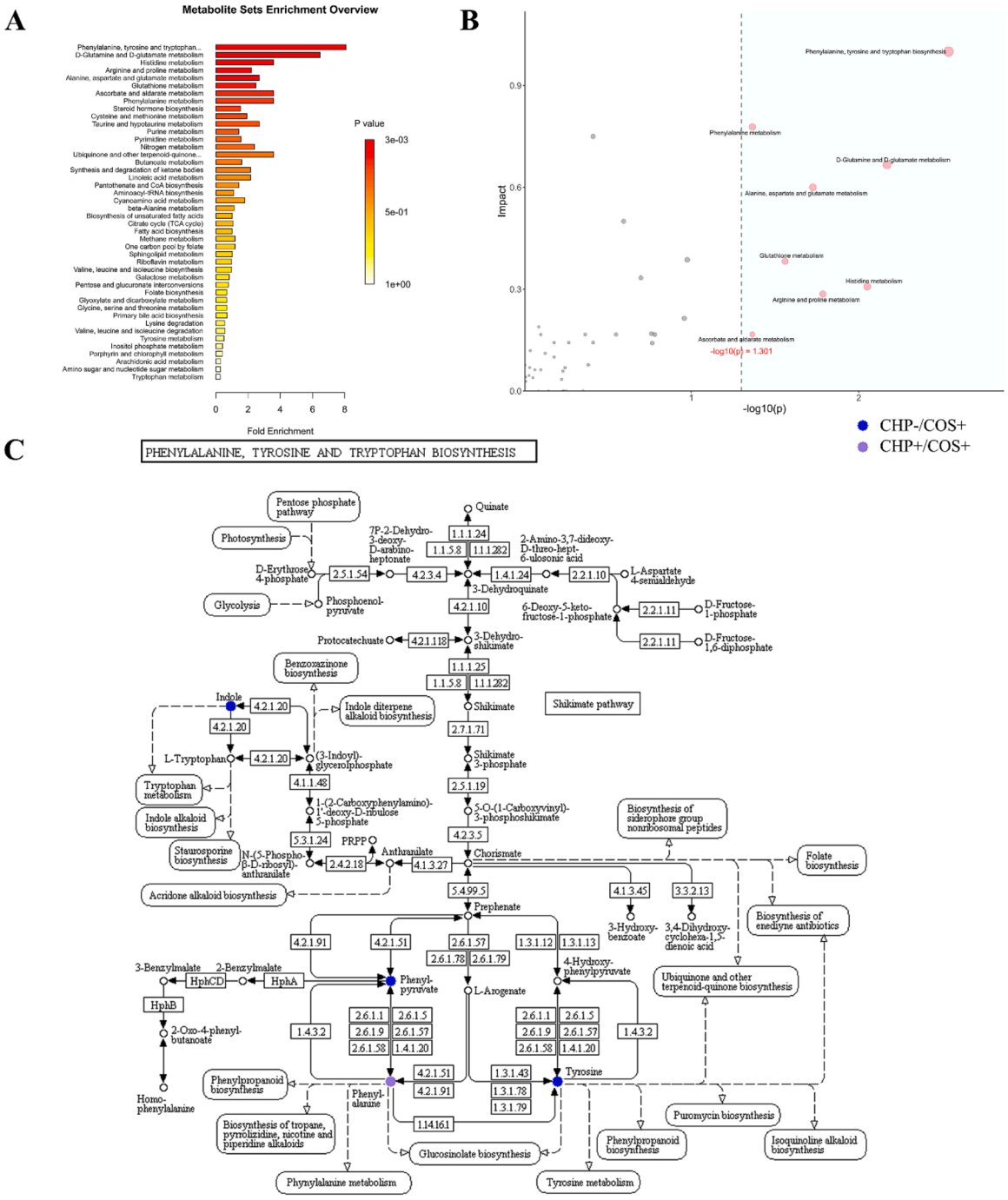

Fig. 8. Metabolic pathways with significant differences between groups and related molecules with significant differences in the pathways. (A) Random forests represent the distribution of metabolic pathways with significant differences between each treatment groups; (B) Bubble plots of metabolic pathways with the largest differential changes between treatment groups; (C) Pathway network with the most differences among the treatment groups and its key molecules with significant differences. The annotation of CHP and COS can be seen in the legend of Fig. 1; n = 5 per group.

compositions of the different treatment groups were highly similar. Because alpha and beta diversity are often used to characterise within-habitat diversity and between-habitat diversity, respectively, these indices may reflect changes in the functional modules of microorganisms.

We also used linear discriminant analysis effect size (LEfSe) to identify bacteria with differences in abundance between groups and samples to identify genera with significantly high abundance among the groups. In the clade diagram, species with no significant difference in abundance are uniformly coloured in yellow and species with significantly different biomarkers are coloured according to the group. The diameter of each circle represents the relative abundance of the taxonomic units. As shown in the figure, the specific microbial species (23 species) in the CHP treatment group were significantly lower than those in the CHP-/COS- group (58 species) ($P < 0.05$), while the remission effect of the CHP+/COS+ group (30 species) was not significant ($P > 0.05$) (Fig. 10A). The same result was confirmed in the histogram of the linear discriminant analysis (LDA) distribution (Fig. S6).

To explore the potential links between relevant environmental factors and microbial communities, we used redundancy analysis (RDA) to summarise the linear relationships between them. As can be seen from Fig. 10B-C, two factors of CHP and COS were positively correlated with

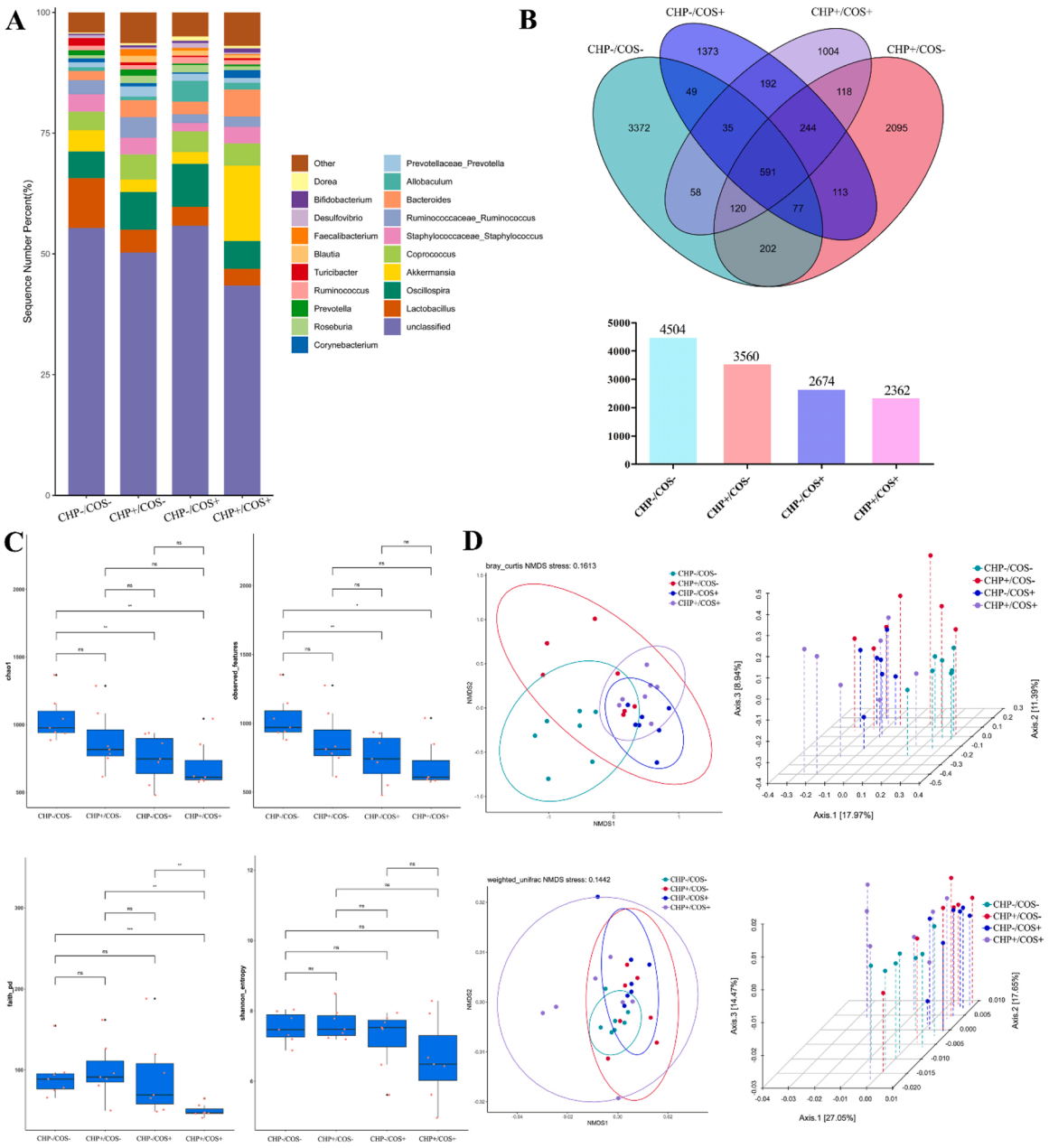

Fig. 9. Changes in the overall structure of the faecal samples of rats in different treatment groups. (A) Microbial composition profiles of each group at the genus level (top 20); (B) Changes in microbial OTUs in the caecal contents of each treatment group were represented using a petal diagram; (C) Alpha-diversity was estimated as changes in Chao1, OTUs, Faith's phylogenetics diversity index, and the Shannon index; (D) Differences in microbial community structure between samples were estimated as changes in Bray Curtis dissimilarity and weighted UniFrac indices in beta-diversity and displayed using principal coordinates analysis (PCoA) and non-metric multidimensional scaling (NMDS) plots. The annotation of CHP and COS can be seen in the legend of Fig. 1; n = 7 per group. $^{*}P < 0.05$, $^{**}P < 0.01$, $^{***}P < 0.001$.

microbial community composition. Moreover, the heatmap also explored the correlation between the two treatments, such as the correlation between bacterial abundance at the genus level and environmental factors CHP and COS. An asterisk (*) indicates a significant correlation with $P < 0.05$, two asterisks (**) indicate $P < 0.01$, and three asterisks (***) denote a strong correlation with $P < 0.001$. As shown in Fig. 10E, there was a significant correlation between both CHP and COS and bacterial abundance, with *Treponema*, *Peptostreptococcaceae_Clostridium*, and *WAL_1855D* showing a strong negative correlation and *Moraxellaceae_Acinetobacter, Enterococcus*, *Anaerostipes*, and *Weissella* showing a strong positive correlation ($P < 0.001$). This suggests a correlation between the two factors of CHP and COS and the abundance of faecal microorganisms. In addition, the strength of the correlation between microbial communities at the genus level was clearly observed in the network analysis. The red line represents a positive correlation, the blue line represents a negative correlation, and the thicker the line, the stronger is the correlation (Fig. 10D). The strongest correlation was observed between the genera in Firmicutes. Among them, the strongest correlation was observed between *Lactobacillus* and other genera. This was consistent with the species abundance shown in Fig. 9A. This suggests that there are potential links between both CHP and COS and microorganisms.

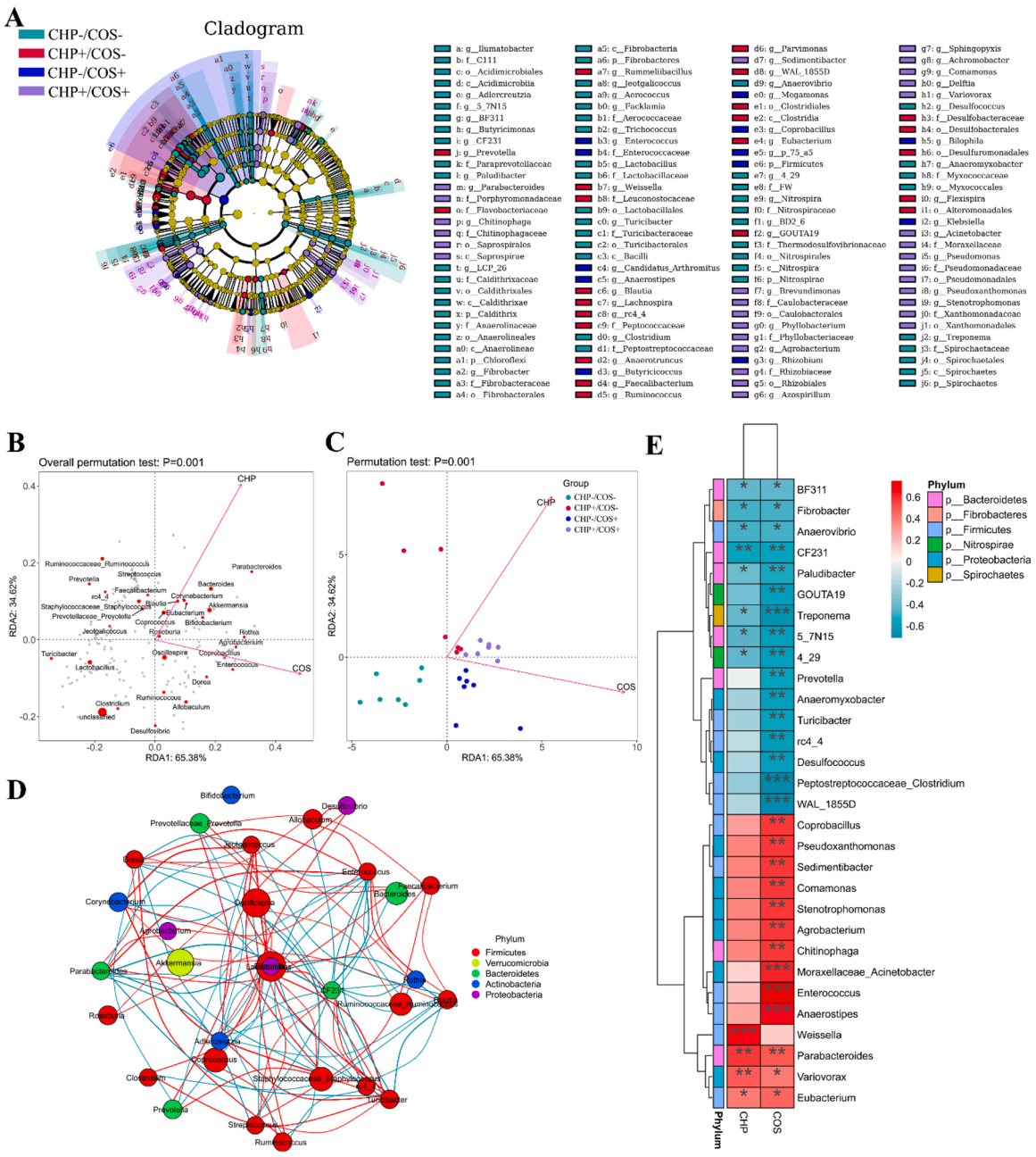

Fig. 10. Comparison of differential microorganisms among different treatment groups and correlation analysis of environmental factors. (A) Biomarkers with significant differences among different treatment groups were represented by an evolutionary branch diagram; (B-C) Using redundancy analysis (RDA) analysis, we explored the regression relationship between CHP and COS and features; (D) Calculate the correlation coefficient of the feature and connected the significantly related feature nodes to draw a network graph; (E) The correlation heatmap was used to explore the correlation between bacterial abundance and environmental factors CHP and COS. The annotation of CHP and COS can be seen in the legend of Fig. 1; n = 7 per group. *$P < 0.05$, **$P < 0.01$, ***$P < 0.001$.

3.11. Potential correlation between the changes of gut microbiota and metabolites

To elucidate the functional correlation between gut microbes and metabolites, a correlation matrix was calculated using Spearman's correlation coefficients between microbes and metabolites, and heat maps were drawn. The red squares represent positive correlations and the blue squares represent negative correlations. Significant correlations were observed between the alterations in metabolites and genus-level gut microbes ($P < 0.05$). The correlations between the top 50 gut microbes and different metabolites are presented in Fig. S7, with 55 microbe-metabolite groups identified as having correlations. For example, the metabolites associated with carbohydrate metabolism [D-Glucose 6-phosphate, D-mannose 1-phosphate, 2-Deoxyribose 5-phosphate, and glutathione (oxidised)] were positively correlated with the abundance of *Ruminococcaceae Ruminococcus* and negatively correlated with the abundance of *Adlercreutzia* and *Weissella*. Lipid metabolism-related metabolites LPC 16:0 and LysoPE 18:0 and the purine metabolite xanthine were significantly negatively correlated with the abundance of *Lachnospira*. In addition, most lipid metabolism-related metabolites (docosahexanoic acid, trans-petroselinic acid, LysoPA 18:0, LPC 18:2, taurolithocholic acid, glycerol 3-phosphate, and docosatrienoic acid) were significantly positively correlated with the abundance of *Bilophila*. In contrast, the glycodeoxycholic acid content was significantly negatively correlated with the abundance of *Bilophila*. The interfering effect of CHP on carbohydrate and lipid metabolism in rats was attributed to

the alteration of gut microbiota indirectly regulated by CHP. Interestingly, some of the metabolic intermediates (D-ribose, stearic acid, D-Gluconic acid, xanthosine, and D-glutamine) showed significant positive correlations with a few genera, such as *Parabacteroides* and *Oscillospira*, and significant negative correlations with many gram-positive bacteria (*Jeotgalicoccus, Bifidobacterium, Turicibacter, Corynebacterium, Lactobacillus,* and *Staphylococcaceae Staphylococcus*); however, the correlation between reduced glutathione and these genera showed an opposite trend. Glutathione (reduced) also showed positive correlations with some bacteria that produce short-chain fatty acids, such as *Butyricimonas* and *Blautia*. In addition, some other metabolites, such as Thromboxane B2, which is a prostaglandin, showed a significant positive correlation with *Odoribacter*, *Sutterella*, *Coprococcus*, and *Desulfovibrio* and a significant negative correlation with *Clostridium* and *Streptococcus*. There was also a significant negative correlation between pantothenate or pantothenic acid, as coenzymes, and *Roseburia*. These results suggest that exposure to CHP leads to significant taxonomic perturbations in the gut microbiome, which are closely associated with alterations in the metabolomic profile, as evidenced by the changes in metabolites associated with multiple gut microbial communities. Therefore, the health risks associated with CHP systems cannot be ignored.

4. Discussion

In this experiment, both the toxicological and environmental significance of CHP were considered in the dose selection. In terms of toxicological significance, 10 mg/kg BW of CHP induced intestinal oxidative stress and decreased AChE activity, which is also 1/15 of the LD50 [52–56]. In terms of environmental significance, we considered both the intake dose of CHP and the environmental concentration. Firstly, in terms of intake dose, the residues of CHP detected in the soybean systems of Anhui, Jilin, and Shandong provinces were between 0.23 and 70.7 mg/kg [57]. Based on the ADFI of 30 g for rats weighing approximately 200 g, it was calculated to range between 0.046 and 14.4 mg of daily intake in rats. The 10 mg/kg BW used in our experiment was the daily intake of 2 mg of CHP by rats, which is also within the upper limit of the detected CHP residue concentration in soybean; Secondly, in terms of concentration selection, crops are the first target of CHP application, while soil and water environments are indirectly exposed to CHP. Since CHP enters animals or humans through residues in food, oral administration of crops is the most appropriate method for ingestion of chlorpyrifos [58]. The concentration of CHP in our formulated corn oil was higher than the maximum concentration detected (70.7 mg/kg) for two reasons: (1) The intestinal tolerance of rats is higher than that of humans [55]; (2) CHP in our experiment is a short-term high dose intake. In the real environment, although CHP is a long-term low dose exposure process, this can lead to a large accumulation of CHP in the body [6,59]. So our dosing method can mimic the relationship of CHP exposure in the environment. Therefore, the selected doses were of environmental and toxicological significance.

In toxicology studies, significant changes in body and organ weight are usually regarded as the most intuitive indicators for evaluating toxic chemicals [60]. Moreover, previous studies have shown that the primary toxic effect of CHP is neurological toxicity [55,61,62]. AChE activity was significantly inhibited in the CHP-treated group in our experiments, which may lead to structural defects in the digestive tract [32]. Moreover, oxidative stress is a major contributor to intestinal tissue damage and intestinal diseases [63]. In pre-experiments, we have found that CHP at this dose can cause intestinal oxidative stress. This corresponds to the changes in gut morphology that we measured. This leads to restricted absorption of nutrients in rats. Moreover, studies have shown that CHP can be rapidly absorbed by mammals, causing damage to the metabolism of tissues and organs [64]. The accumulation of CHP in adipose tissue is the highest among all tissues and organs, leading to weight loss in animals [23]. Moreover, COS not only has a strong ability to protect impaired lipid metabolism [65], but low molecular weight and doses of COS can also enhance the growth rate of monogastric animals by improving the structure and morphology of the small intestine [66]. Therefore, in this study, COS alleviated weight loss in rats by interfering with CHP-induced abnormalities in lipid metabolism and protecting intestinal morphology.

Digestion and absorption of nutrients occur mainly in the brush border membrane and enterocytes of the small intestine [67], which play an important role in material metabolism. Before the experiment, we determined the CHP residues in the ileum tissue, colonic contents, and the proportion between the ileum and colonic contents to determine whether CHP was absorbed by the small intestine or excreted by the body. The results indicate that part of the CHP was absorbed into the body by the small intestine, and part of it was excreted in the faeces. Owing to its good biocompatibility, COS is considered to form a protective film through emulsification in the digestive tract [66], thereby reducing the absorption of CHP in the gastrointestinal tract of rats during growth. Therefore, the COS remission group had more CHP residues in the colonic contents than the CHP group, as measured in our study, because the physical protective effect of COS facilitates the excretion of CHP.

To examine CHP toxicity, many enzyme activities that are important indicators of exogenous contaminant toxicity have been measured in serum [68]. When liver tissue is damaged, the liver cell membrane ruptures and ALT and AST are released into the blood [69]. Therefore, ALT and AST levels are important diagnostic indicators for evaluating the degree of liver cell damage. Studies have also confirmed that OPPs can disturb the balance of enzymatic and non-enzymatic antioxidants in the body, resulting in excessive peroxide generation and the loss of cell membrane integrity [52]. CHP has long been reported to cause hepatotoxicity [70]. In our experiment, CHP caused liver dysfunction, rupture of the hepatocyte membrane, and a large influx of AST from the liver to the blood, resulting in a significant increase in the serum AST content and an imbalance of the AST/ALT ratio, indicating a diseased state in the liver.

In our study, we also observed a decrease in AChE activity and an increase in the amount of ACh in the serum of CHP-treated rats. AChE hydrolyses ACh in central and peripheral cholinergic synapses [62]. CHP has typical neurotoxic effects as an OPP. The mechanism of toxicity involves inhibiting the activity of AChE by phosphorylating its active site, thus causing excessive accumulation of ACh and continuous stimulation of ACh receptors (AChRs) [26]. Synapses formed by vagal nerve branches are the main source of ACh signals in the gastrointestinal tract [71]. Muscarinic receptors (MRs) are closely associated with smooth muscle and digestive gland secretions in the gastrointestinal tract [61]. Moreover, recent studies have shown that these drugs play a key role in influencing neuromodulation and sensory input at the level of chemoreceptor receptors and further influence intestinal activity, which is a key factor inducing functional dyspepsia [72]. In turn, vagal mechanoreceptor terminals stimulate gastric dilatation-sensitive neurons in the ventral medial nucleus of the hypothalamus, which can further modulate neurocentral activity and digestive motility to induce satiety [73]. Thus, the neurotoxic effects of CHP can also interfere with gastrointestinal (GI)tract activity and eating behaviour via the brain-gut axis pathway.

In addition, oxidative stress can also reflect the toxic effects of CHP, manifested as excessive accumulation of peroxidation products (H_2O_2, MDA, etc.) [74] in the body, or altered activity of cellular antioxidants (GPx, GST, CAT, SOD, etc.) [75]. Oxidative stress is caused by ROS or other oxidants in the body that disrupt the balance of oxidative and antioxidant systems, resulting in various diseases. Among these, the antioxidant defence system is the main system associated with the above-mentioned antioxidant enzymes [76]. T-SOD catalyses the conversion of ROS to O_2 and H_2O_2. CAT then catalyses H_2O_2 into O_2 and H_2O without side effects [77–79]. Through this process, the body achieves the protective ability of self-clearing ROS [80]. Therefore, in this experiment, changes in the activity of T-SOD and CAT indirectly

reflected changes in the levels of reactive oxygen species in the body. However, the reason for the lack of change in the ROS content is that the body resists this oxidative imbalance by increasing CAT activity.

In this study, COS significantly inhibited CHP-induced oxidative stress. COS is the only naturally positively charged cationic basic amino oligosaccharide. Not only does it provide a positive charge to free radicals, but, because COS is an oligosaccharide, it also has many active hydroxyl and amino groups [81]. This shows that COS has a high reducing ability, can effectively remove ROS in the body, and improves antioxidant capacity [82]. This has been confirmed by studies showing that COS can effectively increase the gene expression of antioxidant enzymes, such as SOD and GPx [83], which is consistent with our observations. COS itself has antioxidant functions. It relieves the imbalance of the antioxidant system caused by CHP by increasing the expression of nuclear transcription factor Nrf2, the activity of CAT, and other antioxidant enzymes and reduces oxidative stress without the need for the body to adjust itself. Therefore, it is not difficult to understand that, while COS improves the antioxidant status of rats, it avoids the damaging effect of ROS on hepatocyte membranes, thereby effectively preventing the leakage of AST in hepatocytes.

CHP exposure not only disrupts the antioxidant system but also causes immune-related gene expression and histological damage [84]. On the one hand, CHP-mediated mitochondrial oxidative stress stimulates inflammasomal and innate immune responses [85]. However, excessive ROS production due to destruction of the antioxidant system is often accompanied by inflammation and apoptosis [86]. Moreover, NF-κB is extremely sensitive to oxidative stress and plays an important role in stimulating the activation of pro-inflammatory cytokines. TNF-α is necessary for stimulating the activation of IL-1β and IL-6 [87]. The upregulation of these cytokines is directly related to inflammation in animals [88]. Moreover, some studies have shown that NF-κB activation leads to the activation of a large number of pro-inflammatory genes, which in turn triggers the production of excess ROS [86]. This is consistent with the results of our experiments. This indicates that CHP promotes inflammatory responses by activating NF-κB molecules, resulting in over-expression of pro-inflammatory factor genes in the rat duodenum and jejunum, low expression of anti-inflammatory factor genes, and a significant increase in inflammatory cells, thereby aggravating toxicity.

Inflammatory processes are often accompanied by apoptosis. This process is controlled by proteins of the Bcl-2 family, including pro-apoptotic proteins (Bax and Bad) and anti-apoptotic proteins (Bcl-2) [89]. Bcl-2 inhibits ROS formation by inhibiting mitochondrial depolarisation and blocking the mitochondrial pathway [90]. Exposure to CHP shifts the balance between anti-apoptotic and pro-apoptotic proteins toward the pro-apoptotic pathway, which results in a reduction in anti-apoptotic proteins and activation of pro-apoptotic proteins [91]. Some studies have confirmed that CHP promotes apoptosis signalling through increased ROS levels, mitochondrial membrane collapse, and the release of cytochrome C [92]. Caspase-3 activates other caspases and initiates apoptosis. Cytochrome C can also activate caspase-3 and caspase-9 to induce apoptosis [93]. This indicates that CHP exposure is associated with apoptosis, which manifests as increased expression of Bax and Bad genes, downregulation of Bcl-2 expression, and a cascade response of caspase-3 and caspase-9. Moreover, mitochondrial dysfunction and apoptosis often occur at these inflammatory sites [94], similar to the findings of our current study. CHP alters the balance between cellular inflammation and apoptosis by altering the expression of Bcl-2 family proteins and caspases.

Studies have indicated that, when encountering environmental toxicants, the body regulates the intestinal inflammatory response by regulating the secretion of cytokines, thereby destroying the intestinal structure [95]. Intestinal villi are a typical structure in the small intestine, and their structural integrity directly reflects the ability of the small intestine to digest and absorb nutrients [96]. Furthermore, a higher villus/crypt ratio indicates a higher growth rate [66]. In our study, CHP was found to cause tissue damage in the duodenum and jejunum, which is related to changes in the inflammatory factors in the gut. This is also the fundamental reason for the weight loss in CHP-treated rats. If the outer villi of the gut are the first defence barrier against external stimuli, then the tight junction proteins in the inner layer form the second immune barrier [97]. When stimulated by external oxidative stress, the intestinal microenvironment changes, and the concentration of tight junction proteins is reduced, which leads to an increase in intestinal permeability and causes a variety of intestinal diseases, including intestinal inflammation [98]. This suggests that, in our experiments, CHP exposure led to alterations in the intestinal microenvironment of rats, thus causing damage to the villi and reducing the expression of tight junction proteins, which threatens health.

Based on these toxic effects of CHP, it is necessary to select an effective palliative agent. Antioxidant therapy using natural substances is considered an appropriate strategy to improve oxidative stress, inflammation, and apoptosis [31,87]. As a naturally healthy food, COS has remarkable effects on antibacterial, antitumour, and antioxidant processes, immune regulation, and alleviation of inflammation [99] and can be called a natural immune enhancer [100]. COS changes the cell membrane permeability by increasing the number of cationic amines and changing the potential of the cell membrane surface. In addition, electrostatic complexation can be generated between COS and proteins in food, thereby forming COS-protein precipitates. This composite precipitate has various physical properties such as gelling, foaming, and emulsifying [101,102]. Therefore, these precipitates can accumulate on the intestinal surface to form a physical protective film to prevent CHP damage to epithelial cells, thereby reducing the inflammatory response and apoptotic signal of CHP in rats. This plays a crucial role in protecting the integrity and structure of the intestinal barrier.

Metabolomics has been used as an important assay for assessing environmental pollutants and the effects of pollutants on exposed organisms [103–105]. Therefore, intestinal metabolomics was selected for this experiment, which confirmed the strong effect of CHP on the intestinal metabolic capacity of rats and that COS supplementation regulated these impairments. Studies have found that low-dose CHP (as low as 1 pM) can affect fat metabolism and promote obesity [106]; however, the concentration of CHP used (10 mg/kg BW) is higher than the critical value that can promote obesity. We observed a significant decrease in long-chain fatty acid amides and oleamides in the CHP+/COS- group. In addition, oleamide, a fatty acid amide with endocannabinoid properties, has neuroprotective and modulating properties in toxically injured organisms [107] as well as a significant antidepressant effect [108]. However, the oleamide content decreased after CHP treatment, and the addition of COS prevented the decrease in the oleamide content, indicating that the neuroprotective effect of oleamide was reduced after CHP treatment. This also suggests that, in addition to reducing AChE activity, CHP has other neurotoxic mechanisms triggered by reducing the oleamide content, and COS has an effective protective effect on this mechanism.

Among these metabolites, amino acids are key factors in the biosynthesis of important molecules in the immune response, which are related to their important cellular functions and role as precursors to hormones and enzymes [109]. Unlike tyrosine, D-tryptophan is an essential amino acid. Although it is not involved in protein synthesis [110], it has special physiological functions such as inhibiting bacterial growth and bacterial biofilm development [111]. However, once a deficiency occurs, the harm caused by these two amino acids in the body cannot be ignored. Tryptophan can also be converted into hormones and neurotransmitters through biochemical reactions, such as melatonin through hydroxylation reactions [112], and the synthesis of the important neurotransmitter 5-hydroxytryptamine (5-HT) [113]. Thus, after CHP treatment, the endocrine function and nervous system are in a state of imbalance based on the detection of the lack of some amino acids or the abnormality of related amino acid metabolic pathways.

Gut microbiota is currently considered to play a role in regulating

intestinal motility, maintaining the integrity of the intestinal epithelial barrier, and regulating the normal development and activity of the immune system [114,115]. Therefore, structural changes are considered important indicators for assessing the biological effects of contaminants. Although recent studies have demonstrated that CHP affects lipid metabolism [106], the role of gut microbiota is not well understood. Numerous studies have shown that *Lactobacillus* is involved in lipid metabolism and is closely related to obesity [116–118]. However, we found that the CHP-induced decrease in the relative abundance of *Lactobacillus* did not cause obesity in rats, but decreased body weight. This is because the concentration of CHP (10 mg/kg BW) exceeds the highest concentration that causes obesity (1 pM), resulting in a more severe destruction of the intestinal epithelial barrier than a greater change in the relative abundance of *Lactobacillus*. In addition, decreased gut microbiota diversity and richness are important indicators of gut inflammation and oxidative stress [119]. Several environmental pollutants have been shown to reduce gut microbiota diversity, alter gut composition, and ultimately negatively impact gut microbiota [120]. Therefore, on the one hand, CHP causes intestinal inflammation and oxidative damage directly, and on the other hand, it can be achieved indirectly by reducing microbial diversity and richness. However, COS cannot alleviate changes in microbial diversity and abundance because its alleviating effect on intestinal damage is a direct result of the formation of a physical protective layer and is not achieved by the modulation of microorganisms in the intestinal environment.

To further demonstrate that CHP alters intestinal homoeostasis by altering the relationship between metabolites and gut microbial abundance, we performed functional correlation analysis between gut bacteria and metabolites at the genus level. We found a significant correlation between CHP-altered metabolites and intestinal flora. Interestingly, we found that multiple carbohydrate metabolites correlated with the abundance of family including *Lactobacillus* (*Weissella*) and *Coriobacteriia* (*Adlercreutzia*). Early studies on *Weissella* and *Adlercreutzia* cells detected monosaccharides such as ribose, galactose, and glucose as their main carbohydrate sources, and they use monosaccharide metabolism to obtain the intermediate product glucose 6-phosphate, which is necessary for cellular activity [121,122]. Moreover, the *Adlercreutzia* cells were able to produce arginine dihydrolase and showed weak responses to the production of arginine arylamidase and leucine arylamidase [123]. Not surprisingly, the results provide further evidence for the metabolic pathway in Fig. 8A, which also suggests that altered intestinal metabolic function is attributed to indirect regulation of CHP. We also found a strong correlation between probiotics inhabiting the GI tract, such as *Lactobacillus* and *Bifidobacterium*, and the small molecules intermediate in most metabolic pathways. In support of this, previous studies have shown that host-microbe interactions can influence host metabolism and induce metabolic changes similar to the metabolic syndrome [124]. Here, these probiotics affect host metabolism mainly just by playing an important probiotic role through the protection against gut microbiota imbalance and immune dysregulation, among other pathways [125]. Thus, from these aspects it can be concluded that there is an inextricable link between host gut metabolic function and microorganisms.

In the present study, we applied COS to alleviate the adverse effects of CHP that have not been reported. Notably, Spearman analysis to predict the relationship between CHP-induced changes in intestinal microbial structure and metabolic differences demonstrated that changes between the two were significantly correlated. Other results showed that the CHP+/COS+ group showed excellent relief of intestinal inflammation, apoptosis, barrier integrity, and metabolic function compared with the CHP group, and the relief was largely consistent with that of the control group. These results are also unprecedented in previous studies. However, it is still unknown whether COS still has the same effect on rats chronically exposed to CHP, so further systematic studies are needed.

5. Conclusions

In conclusion, after exposure to CHP, the rat duodenum and jejunum experienced remarkable oxidative damage, inflammation, apoptosis, and gut barrier damage, which led to intestinal digestion and absorption disorders and, in turn, adversely affected the growth performance of the rats. Because COS itself has the physical properties of emulsification and film formation, coupled with its physiological properties, such as antioxidant, anti-inflammatory, and anti-apoptotic properties, after pretreatment with COS as a protective agent, a gel protective layer was formed on the intestinal epithelium. This hindered the invasive effect of CHP on the intestinal tract of the rats and simultaneously ensured normal intestinal metabolism. This indicates that COS effectively alleviates intestinal barrier damage caused by CHP through physical action, rather than by changing the diversity of gut microbes. Therefore, according to our findings, COS has great potential for application in removing and alleviating intestinal dysfunction and damage caused by environmental residual CHP.

Environmental implication

Chlorpyrifos (CHP) is the most widely used organophosphorus insecticide worldwide. Since it is a moderately toxic pesticide, it has been abused in production. The CHP emission remaining on the plant surface enters the ecosystem cycle through rainwater runoff, causing unavoidable toxicological effects on non-target organisms. Currently, CHP residues are found in soil, water, humans, and animals. Therefore, it is urgent to explore a method to remove and mitigate the toxicological effects of CHP exposure on non-target organisms.

CRediT authorship contribution statement

Zhenlong Wu: Conceived, designed, and directed the work. **Huiyang Fu**: Conducted the experiments, data analysis, and writing. **Haozhen Liu, Yao Ge, and Peng Tan**: Experimental data processing and analysis. **Yinfeng Chen**: Spearman correlation analysis. **Jun Bai, Zhaolai Dai, and Ying Yang**: Writing, review and editing.

Declaration of Competing Interest

The authors declare that they have no known competing financial interests or personal relationships that could have appeared to influence the work reported in this paper.

Data availability

The authors do not have permission to share data.

Acknowledgements

This work was supported by the National Key R&D Program of China (Nos. 2022YFF1100102), National Natural Science Foundation of China (Nos. 31625025), and the 2115 Talent Development Program of China Agricultural University.

Appendix A. Supplementary material

Supplementary data associated with this article can be found in the online version at doi:10.1016/j.jhazmat.2022.130669.

References

[1] Gilani, R.A., Rafique, M., Rehman, A., Munis, M.F., Rehman, S.U., Chaudhary, H. J., 2016. Biodegradation of chlorpyrifos by bacterial genus Pseudomonas. J Basic Microbiol 56, 105–119.

[2] Joly Condette, C., Djekkoun, N., Reygner, J., Depeint, F., Delanaud, S., Rhazi, L., et al., 2022. Effect of daily co-exposure to inulin and chlorpyrifos on selected microbiota endpoints in the SHIME(R) model. Environ Pollut 302, 118961.
[3] Djekkoun, N., Depeint, F., Guibourdenche, M., El Khayat El Sabbouri, H., Corona, A., Rhazi, L., et al., 2022. Chronic perigestational exposure to chlorpyrifos induces perturbations in gut bacteria and glucose and lipid markers in female rats and their offspring. Toxics 10.
[4] Chiu, K.C., Sisca, F., Ying, J.H., Tsai, W.J., Hsieh, W.S., Chen, P.C., et al., 2021. Prenatal chlorpyrifos exposure in association with PPARgamma H3K4me3 and DNA methylation levels and child development. Environ Pollut 274, 116511.
[5] John, E.M., Shaike, J.M., 2015. Chlorpyrifos: pollution and remediation. Environ Chem Lett 13, 269–291.
[6] Sang, C., Sorensen, P.B., An, W., Andersen, J.H., Yang, M., 2020. Chronic health risk comparison between China and Denmark on dietary exposure to chlorpyrifos. Environ Pollut 257, 113590.
[7] Pignati, W.A., Lima, F.A.Nd.S., Lara, S.Sd, Correa, M.L.M., Barbosa, J.R., Leão, L. Hd.C., et al., 2017. Distribuição espacial do uso de agrotóxicos no Brasil: uma ferramenta para a Vigilância em Saúde. Ciênc Saúde Coletiva 22, 3281–3293.
[8] Chishti, Z., Hussain, S., Arshad, K.R., Khalid, A., Arshad, M., 2013. Microbial degradation of chlorpyrifos in liquid media and soil. J Environ Manag 114, 372–380.
[9] Falfushynska, H., Khatib, I., Kasianchuk, N., Lushchak, O., Horyn, O., Sokolova, I. M., 2022. Toxic effects and mechanisms of common pesticides (Roundup and chlorpyrifos) and their mixtures in a zebrafish model (Danio rerio). Sci Total Environ 833, 155236.
[10] Bilaro, J.S., Materu, S.F., Temba, B.A., 2022. Dietary risk assessment of selected organophosphorus and pyrethoid pesticide residues in fresh harvested tomatoes at Makambako Town, Njombe region, Tanzania. Food Addit Contam Part B 1–9.
[11] Calderon, R., García-Hernández, J., Palma, P., Leyva-Morales, J.B., Zambrano-Soria, M., Bastidas-Bastidas, P.J., et al., 2022. Assessment of pesticide residues in vegetables commonly consumed in Chile and Mexico: Potential impacts for public health. J Food Compos Anal 108.
[12] Bhatnagar, A., Dave, R., Jindal, T., Virdi, J.S., 2022. An intensive study on pesticides contamination and its removal in fruits and vegetables collected from Ghaziabad, India. J Exp Biol Agric Sci 10, 104–116.
[13] Anbarasan, R., Jaspin, S., Bhavadharini, B., Pare, A., Pandiselvam, R., Mahendran, R., 2022. Chlorpyrifos pesticide reduction in soybean using cold plasma and ozone treatments. LWT 159.
[14] Uniyal, S., Sharma, R.K., Kondakal, V., 2021. New insights into the biodegradation of chlorpyrifos by a novel bacterial consortium: process optimization using general factorial experimental design. Ecotoxicol Environ Saf 209, 111799.
[15] Li, D., Huang, Q., Lu, M., Zhang, L., Yang, Z., Zong, M., et al., 2015. The organophosphate insecticide chlorpyrifos confers its genotoxic effects by inducing DNA damage and cell apoptosis. Chemosphere 135, 387–393.
[16] Eissa, F., Al-Sisi, M., Ghanem, K., 2021. Occurrence, human health, and ecotoxicological risk assessment of pesticides in surface waters of the River Nile's Rosetta Branch, Egypt. Environ Sci Pollut Res Int 28, 55511–55525.
[17] Xiao, J., Ma, J., Wang, F., Xu, X., Liao, M., Shi, Y., et al., 2021. Effect of decocting on the pesticide residues in Paeoniae radix lactiflora and corresponding exposure risk assessment. Environ Sci Pollut Res 28, 16655–16662.
[18] Pal, P., Shah, P., 2008. Effect of storage and processing on dissipation of five insecticides on wheat. Pestic Res J 20, 253–258.
[19] Liang, Y., Duan, J., Gao, Q., Li, Y., Zhang, Z., 2022. Effect of Chinese steamed bun and bread processing on pesticide residues in wheat flour. Food Prod Process Nutr 4.
[20] Albasher, G., Albrahim, T., Alsultan, N., Alfaraj, S., Alharthi, M.S., Kassab, R.B., et al., 2020. Moneim, Red beetroot extract mitigates chlorpyrifos-induced reprotoxicity associated with oxidative stress, inflammation, and apoptosis in rats. Environ Sci Pollut Res Int 27, 3979–3991.
[21] Huang, Y.F., Pan, W.C., Tsai, Y.A., Chang, C.H., Chen, P.J., Shao, Y.S., et al., 2017. Concurrent exposures to nonylphenol, bisphenol A, phthalates, and organophosphate pesticides on birth outcomes: a cohort study in Taipei, Taiwan. Sci Total Environ 607–608, 1126–1135.
[22] U. EPA. Chlorpyrifos: preliminary human health risk assessment forregistration review. US Environmental Protection Agency Washington, DC, USA; 2011.
[23] Ubaid Ur Rahman, H., Asghar, W., Nazir, W., Sandhu, M.A., Ahmed, A., Khalid, N., 2021. A comprehensive review on chlorpyrifos toxicity with special reference to endocrine disruption: evidence of mechanisms, exposures and mitigation strategies. Sci Total Environ 755, 142649.
[24] Fang, B., Li, J.W., Zhang, M., Ren, F.Z., Pang, G.F., 2018. Chronic chlorpyrifos exposure elicits diet-specific effects on metabolism and the gut microbiome in rats. Food Chem Toxicol Int J Publ Br Ind Biol Res Assoc 111, 144–152.
[25] Ismail, A.A., Hendy, O., Abdel Rasoul, G., Olson, J.R., Bonner, M.R., Rohlman, D. S., 2021. Acute and cumulative effects of repeated exposure to chlorpyrifos on the liver and kidney function among Egyptian adolescents. Toxics 9, 137.
[26] Fu, H., Tan, P., Wang, R., Li, S., Liu, H., Yang, Y., et al., 2022. Advances in organophosphorus pesticides pollution: current status and challenges in ecotoxicological, sustainable agriculture, and degradation strategies. J Hazard Mater 424, 127494.
[27] Aboubakr, M., Elshafae, S.M., Abdelhiee, E.Y., Fadl, S.E., Soliman, A., Abdelkader, A., et al., 2021. Antioxidant and anti-inflammatory potential of thymoquinone and lycopene mitigate the chlorpyrifos-induced toxic neuropathy. Pharmaceuticals 14.
[28] Seth, E., Chopra, M., 2022. Neuroprotective efficacy of berberine following developmental exposure to chlorpyrifos in F1 generation of Wistar rats: apoptosis-autophagy interplay. Sci Total Environ 834, 155292.
[29] Hassan, M.A., El Bohy, K.M., El Sharkawy, N.I., Imam, T.S., El-Metwally, A.E., Hamed Arisha, A., et al., 2021. Iprodione and chlorpyrifos induce testicular damage, oxidative stress, apoptosis and suppression of steroidogenic- and spermatogenic-related genes in immature male albino rats. Andrologia 53, e13978.
[30] Guibourdenche, M., El Khayat El Sabbouri, H., Bonnet, F., Djekkoun, N., Khorsi-Cauet, H., Corona, A., et al., 2021. Perinatal exposure to chlorpyrifos and/or a high-fat diet is associated with liver damage in male rat offspring. Cells Dev 166, 203678.
[31] Kianpour, F., Mohseni, M., Beigmohamadi, M., Yazdinezhad, A., Ramazani, A., Hosseini, M.J., et al., 2021. The protective effects of Ziziphora tenuior L. against chlorpyrifos induced toxicity: involvement of inflammatory and cell death signaling pathway. J Ethnopharmacol 272, 113959.
[32] Guibourdenche, M., El Khayat El Sabbouri, H., Djekkoun, N., Khorsi-Cauet, H., Bach, V., Anton, P.M., et al., 2021. Programming of intestinal homeostasis in male rat offspring after maternal exposure to chlorpyrifos and/or to a high fat diet. Sci Rep 11, 11420.
[33] Miller, D.R., McClain, E.S., Dodds, J.N., Balinski, A., May, J.C., McLean, J.A., et al., 2021. Chlorpyrifos disrupts acetylcholine metabolism across model blood-brain barrier. Front Bioeng Biotechnol 9, 622175.
[34] Zhao, X.P., Liu, J., Sui, Z.J., Xu, M.J., Zhu, Z.Y., 2022. Preparation and antibacterial effect of chitooligosaccharides monomers with different polymerization degrees from crab shell chitosan by enzymatic hydrolysis. Biotechnol Appl Biochem.
[35] Ouyang, A., Wang, H., Su, J., Liu, X., 2021. Mannose receptor mediates the activation of chitooligosaccharides on blunt snout bream (Megalobrama amblycephala) macrophages. Front Immunol 12, 686846.
[36] Hu, H., Xia, H., Zou, X., Li, X., Zhang, Z., Yao, X., et al., 2021. N-acetyl-chitooligosaccharide attenuates inflammatory responses by suppression of NF-κB signaling, MAPK and NLRP3 inflammasome in macrophages. J Funct Foods 78, 104364.
[37] Han, K., Kwon, I., Lohakare, J., Heo, S., Chae, B., 2007. Chito-oligosaccharides as an alternative to antimicrobials in improving performance, digestibility and microbial ecology of the gut in weanling pigs. Asian-Australas J Anim Sci 20, 556–562.
[38] Suthongsa, S., Pichyangkura, R., Kalandakanond-Thongsong, S., Thongsong, B., 2017. Effects of dietary levels of chito-oligosaccharide on ileal digestibility of nutrients, small intestinal morphology and crypt cell proliferation in weaned pigs. Livest Sci 198, 37–44.
[39] Liu, P., Piao, X., Kim, S., Wang, L., Shen, Y., Lee, H., et al., 2008. Effects of chito-oligosaccharide supplementation on the growth performance, nutrient digestibility, intestinal morphology, and fecal shedding of Escherichia coli and Lactobacillus in weaning pigs. J Anim Sci 86, 2609–2618.
[40] Yang, C., Ferket, P., Hong, Q., Zhou, J., Cao, G., Zhou, L., et al., 2012. Effect of chito-oligosaccharide on growth performance, intestinal barrier function, intestinal morphology and cecal microflora in weaned pigs. J Anim Sci 90, 2671–2676.
[41] Zhao, P., Piao, X., Zeng, Z., Li, P., Xu, X., Wang, H., 2017. Effect of Forsythia suspensa extract and chito-oligosaccharide alone or in combination on performance, intestinal barrier function, antioxidant capacity and immune characteristics of weaned piglets. Anim Sci J 88, 854–862.
[42] Thongsong, B., Suthongsa, S., Pichyangkura, R., Kalandakanond-Thongsong, S., 2018. Effects of chito-oligosaccharide supplementation with low or medium molecular weight and high degree of deacetylation on growth performance, nutrient digestibility and small intestinal morphology in weaned pigs. Livest Sci 209, 60–66.
[43] Walsh, A., Sweeney, T., Bahar, B., Flynn, B., O'Doherty, J., 2012. The effect of chitooligosaccharide supplementation on intestinal morphology, selected microbial populations, volatile fatty acid concentrations and immune gene expression in the weaned pig. Anim Int J Anim Biosci 6, 1620–1626.
[44] Xiao, D., Wang, Y., Liu, G., He, J., Qiu, W., Hu, X., et al., 2014. Effects of chitosan on intestinal inflammation in weaned pigs challenged by enterotoxigenic Escherichia coli. PLoS One 9, e104192.
[45] Lodhi, G., Kim, Y.-S., Hwang, J.-W., Kim, S.-K., Jeon, Y.-J., Je, J.-Y., et al., 2014. Chitooligosaccharide and its derivatives: preparation and biological applications. BioMed Res Int (2014).
[46] Joly Condette, C., Bach, V., Mayeur, C., Gay-Queheillard, J., Khorsi-Cauet, H., 2015. Chlorpyrifos exposure during perinatal period affects intestinal microbiota associated with delay of maturation of digestive tract in rats. J Pediatr Gastroenterol Nutr 61, 30–40.
[47] Joly Condette, C., Khorsi-Cauet, H., Morliere, P., Zabijak, L., Reygner, J., Bach, V., et al., 2014. Increased gut permeability and bacterial translocation after chronic chlorpyrifos exposure in rats. PLoS One 9, e102217.
[48] Li, J.W., Fang, B., Pang, G.F., Zhang, M., Ren, F.Z., 2019. Age- and diet-specific effects of chronic exposure to chlorpyrifos on hormones, inflammation and gut microbiota in rats. Pestic Biochem Physiol 159, 68–79.
[49] Singh, V., Panwar, R., 2014. In vivo antioxidative and neuroprotective effect of 4-Allyl-2-methoxyphenol against chlorpyrifos-induced neurotoxicity in rat brain. Mol Cell Biochem 388, 61–74.
[50] Jiang, Y., Fu, C., Liu, G., Guo, J., Su, Z., 2018. Cholesterol-lowering effects and potential mechanisms of chitooligosaccharide capsules in hyperlipidemic rats. Food Nutr Res 62.

[51] Zhang, H., Zhang, S., Wang, L., Liu, X., Wu, Y., 2018. Chitooligosaccharide guanidine inhibits high glucose-induced activation of DAG/PKC pathway by regulating expression of GLUT2 in type 2 diabetic nephropathy rats. J Funct Foods 41, 41–47.
[52] Barski, D., Spodniewska, A., 2018. Effect of chlorpyrifos and enrofloxacin on selected enzymes in rats. Pol J Vet Sci 21, 39–46.
[53] Li, J., Pang, G., Ren, F., Fang, B., 2019. Chlorpyrifos-induced reproductive toxicity in rats could be partly relieved under high-fat diet. Chemosphere 229, 94–102.
[54] Richardson, J.R., Chambers, J.E., 2005. Effects of repeated oral postnatal exposure to chlorpyrifos on cholinergic neurochemistry in developing rats. Toxicol Sci Off J Soc Toxicol 84, 352–359.
[55] Wang, H.P., Liang, Y.J., Sun, Y.J., Hou, W.Y., Chen, J.X., Long, D.X., et al., 2014. Subchronic neurotoxicity of chlorpyrifos, carbaryl, and their combination in rats. Environ Toxicol 29, 1193–1200.
[56] Huang, H.M., Pai, M.H., Liu, J.J., Yeh, S.L., Hou, Y.C., 2019. Effects of dietary exposure to chlorpyrifos on immune cell populations and inflammatory responses in mice with dextran sulfate sodium-induced colitis. Food Chem Toxicol Int J Publ Br Ind Biol Res Assoc 131, 110596.
[57] Tong, Z., Sun, M., Zhou, Z., Dong, X., Hu, B., Duan, J., 2021. The fate and effect of chlorpyrifos and lambda-cyhalothrin in soybean (Glycine max L. Merril) field. Ecotoxicol Environ Saf 209, 111861.
[58] Tripathi, S., Srivastav, A.K., 2010. Nephrotoxicity induced by long-term oral administration of different doses of chlorpyrifos. Toxicol Ind Health 26, 439–447.
[59] Dai, P., Jack, C.J., Mortensen, A.N., Bustamante, T.A., Bloomquist, J.R., Ellis, J. D., 2019. Chronic toxicity of clothianidin, imidacloprid, chlorpyrifos, and dimethoate to Apis mellifera L. larvae reared in vitro. Pest Manag Sci 75, 29–36.
[60] Khalaf, A.A., Ogaly, H.A., Ibrahim, M.A., Abdallah, A.A., Zaki, A.R., Tohamy, A. F., 2022. The reproductive injury and oxidative testicular toxicity induced by chlorpyrifos can be restored by zinc in male rats. Biol Trace Elem Res 200, 551–559.
[61] Todd, S.W., Lumsden, E.W., Aracava, Y., Mamczarz, J., Albuquerque, E.X., Pereira, E.F.R., 2020. Gestational exposures to organophosphorus insecticides: From acute poisoning to developmental neurotoxicity. Neuropharmacology 180, 108271.
[62] Siqueira, A.A., Cunha, A.F., Marques, G.L.M., Felippe, I.S.A., Minassa, V.S., Gramelich, T., et al., 2019. Atropine counteracts the depressive-like behaviour elicited by acute exposure to commercial chlorpyrifos in rats. Neurotoxicol Teratol 71, 6–15.
[63] Shi, Y., Li, J., Yang, P., Niu, Z., Wei, L., Chen, L., et al., 2020. Colchicine increases intestinal permeability, suppresses inflammatory responses, and alters gut microbiota in mice. Toxicol Lett 334, 66–77.
[64] Ozturk Kurt, B., Konukoglu, D., Kalayci, R., Ozdemir, S., 2022. Investigation of the protective role of selenium in the changes caused by chlorpyrifos in trace elements, biochemical and hematological parameters in rats. Biol Trace Elem Res 200, 228–237.
[65] Sarkar, S., Das, D., Dutta, P., Kalita, J., Wann, S.B., Manna, P., 2020. Chitosan: a promising therapeutic agent and effective drug delivery system in managing diabetes mellitus. Carbohydr Polym 247, 116594.
[66] Miao, Z., Liu, Y., Guo, L., Zhao, W., Zhang, J., 2020. Effects of dietary chitosan on growth rate, small intestinal morphology, nutrients apparent utilization and digestive enzyme activities of growing Huoyan geese. Anim Int J Anim Biosci 14, 2635–2641.
[67] Zhang, Y., Tan, P., Zhao, Y., Ma, X., 2022. Enterotoxigenic Escherichia coli: intestinal pathogenesis mechanisms and colonization resistance by gut microbiota. Gut Microbes 14, 2055943.
[68] Geyikoglu, F., Turkez, H., Bakir, T.O., Cicek, M., 2013. The genotoxic, hepatotoxic, nephrotoxic, haematotoxic and histopathological effects in rats after aluminium chronic intoxication. Toxicol Ind Health 29, 780–791.
[69] Yener, Z., Celik, I., Ilhan, F., Bal, R., 2009. Effects of Urtica dioica L. seed on lipid peroxidation, antioxidants and liver pathology in aflatoxin-induced tissue injury in rats. Food Chem Toxicol Int J Publ Br Ind Biol Res Assoc 47, 418–424.
[70] Abolaji, A.O., Awogbindin, I.O., Adedara, I.A., Farombi, E.O., 2017. Insecticide chlorpyrifos and fungicide carbendazim, common food contaminants mixture, induce hepatic, renal, and splenic oxidative damage in female rats. Hum Exp Toxicol 36, 483–493.
[71] Tolaymat, M., Sundel, M.H., Alizadeh, M., Xie, G., Raufman, J.P., 2021. Potential role for combined subtype-selective targeting of M1 and M3 muscarinic receptors in gastrointestinal and liver diseases. Front Pharmacol 12, 786105.
[72] Gaman, A., Kuo, B., 2008. Neuromodulatory processes of the brain-gut axis. Neuromodulation 11, 249–259.
[73] Sun, X., Tang, M., Zhang, J., Chen, J.D., 2006. Excitatory effects of gastric electrical stimulation on gastric distension responsive neurons in ventromedial hypothalamus (VMH) in rats. Neurosci Res 55, 451–457.
[74] Badraoui, R., Ben-Nasr, H., Bardakci, F., Rebai, T., 2020. Pathophysiological impacts of exposure to an endocrine disruptor (tetradifon) on alpha-amylase and lipase activities associated metabolic disorders. Pestic Biochem Physiol 167, 104606.
[75] Saoudi, M., Badraoui, R., Rahmouni, F., Jamoussi, K., El Feki, A., 2021. Antioxidant and protective effects of artemisia campestris essential oil against chlorpyrifos-induced kidney and liver injuries in rats. Front Physiol 12, 618582.
[76] Yuan, X.Y., Jiang, G.Z., Wang, C.C., Abasubong, K.P., Zou, Q., Zhou, Y.Y., et al., 2019. Effects of partial replacement of fish meal by yeast hydrolysate on antioxidant capability, intestinal morphology, and inflammation-related gene expression of juvenile Jian carp (Cyprinus carpio var. Jian). Fish Physiol Biochem 45, 187–197.
[77] Yang, S., He, K., Yan, T., Wu, H., Zhou, J., Zhao, L., et al., 2019. Effect of starvation and refeeding on oxidative stress and antioxidant defenses in Yangtze sturgeon (Acipenser dabryanus). Fish Physiol Biochem 45, 987–995.
[78] Araújo, R.S., Sousa, K.R.S., Sousa, F.C.B., Oliveira, A.C., Dourado, L.R.B., Guimarães, S.E.F., et al., 2019. Effect of glycerin supplementation on the expression of antioxidant and mitochondrial genes in broilers. Anim Prod Sci 59, 408.
[79] Ribeiro, C.C.D., Silva, R.M., Campanholo, V., Ribeiro, D.A., Ribeiro Paiotti, A.P., Forones, N.M., 2018. Effects of grape juice in superoxide dismutase and catalase in colorectal cancer carcinogenesis induced by azoxymethane. Asian Pac J Cancer Prev APJCP 19, 2839–2844.
[80] Jovanovic-Galovic, A., Blagojevic, D.P., Grubor-Lajsic, G., Worland, R., Spasic, M. B., 2004. Role of antioxidant defense during different stages of preadult life cycle in European corn borer (Ostrinia nubilalis, Hubn.): diapause and metamorphosis. Arch Insect Biochem Physiol 55, 79–89.
[81] Liang, S., Sun, Y., Dai, X., 2018. A review of the preparation, analysis and biological functions of chitooligosaccharide. Int J Mol Sci 19.
[82] Kim, K.W., Thomas, R.L., 2007. Antioxidative activity of chitosans with varying molecular weights. Food Chem 101, 308–313.
[83] Ngo, D.-H., Qian, Z.-J., Vo, T.-S., Ryu, B., Ngo, D.-N., Kim, S.-K., 2011. Antioxidant activity of gallate-chitooligosaccharides in mouse macrophage RAW264.7 cells. Carbohydr Polym 84, 1282–1288.
[84] Ali, M., Majid, M., Hussain, I., Kali, S., Naz, T., Niazi, M.B.K., et al., 2020. Chlorpyrifos mediated oxidative damage and histopathological alterations in freshwater fish Oncorhynchus mykiss in Northern Pakistan. Aquac Res 51, 4583–4594.
[85] Jang, Y., Lee, A.Y., Jeong, S.H., Park, K.H., Paik, M.K., Cho, N.J., et al., 2015. Chlorpyrifos induces NLRP3 inflammasome and pyroptosis/apoptosis via mitochondrial oxidative stress in human keratinocyte HaCaT cells. Toxicology 338, 37–46.
[86] Zhao, H., Wang, Y., Liu, Y., Yin, K., Wang, D., Li, B., et al., 2021. ROS-induced hepatotoxicity under cypermethrin: involvement of the crosstalk between Nrf2/Keap1 and NF-kappaB/ikappaB-alpha pathways regulated by proteasome. Environ Sci Technol 55, 6171–6183.
[87] Kucukler, S., Comakli, S., Ozdemir, S., Caglayan, C., Kandemir, F.M., 2021. Hesperidin protects against the chlorpyrifos-induced chronic hepato-renal toxicity in rats associated with oxidative stress, inflammation, apoptosis, autophagy, and up-regulation of PARP-1/VEGF. Environ Toxicol 36, 1600–1617.
[88] De Anna, J.S., Castro, J.M., Darraz, L.A., Elias, F.D., Carcamo, J.G., Luquet, C.M., 2021. Exposure to hydrocarbons and chlorpyrifos alters the expression of nuclear receptors and antioxidant, detoxifying, and immune response proteins in the liver of the rainbow trout, Oncorhynchus mykiss. Ecotoxicol Environ Saf 208, 111394.
[89] Turk, E., Kandemir, F.M., Yildirim, S., Caglayan, C., Kucukler, S., Kuzu, M., 2019. Protective effect of hesperidin on sodium arsenite-induced nephrotoxicity and hepatotoxicity in rats. Biol Trace Elem Res 189, 95–108.
[90] Cupic Miladinovic, D., Prevendar Crnic, A., Pekovic, S., Dacic, S., Ivanovic, S., Santibanez, J.F., et al., 2021. Recovery of brain cholinesterases and effect on parameters of oxidative stres and apoptosis in quails (Coturnix japonica) after chlorpyrifos and vitamin B1 administration. Chem Biol Interact 333, 109312.
[91] Albasher, G., Almeer, R., Al-Otibi, F.O., Al-Kubaisi, N., Mahmoud, A.M., 2019. Ameliorative effect of Beta vulgaris root extract on chlorpyrifos-induced oxidative stress, inflammation and liver injury in rats. Biomolecules 9.
[92] Abolaji, A.O., Ojo, M., Afolabi, T.T., Arowoogun, M.D., Nwawolor, D., Farombi, E.O., 2017. Protective properties of 6-gingerol-rich fraction from Zingiber officinale (Ginger) on chlorpyrifos-induced oxidative damage and inflammation in the brain, ovary and uterus of rats. Chem Biol Interact 270, 15–23.
[93] Eldutar, E., Kandemir, F.M., Kucukler, S., Caglayan, C., 2017. Restorative effects of Chrysin pretreatment on oxidant-antioxidant status, inflammatory cytokine production, and apoptotic and autophagic markers in acute paracetamol-induced hepatotoxicity in rats: an experimental and biochemical study. J Biochem Mol Toxicol 31.
[94] Zhao, Y., Fang, C., Jin, C., Bao, Z., Yang, G., Jin, Y., 2022. Catechin from green tea had the potential to decrease the chlorpyrifos induced oxidative stress in larval zebrafish (Danio rerio). Pestic Biochem Physiol 182, 105028.
[95] Luissint, A.C., Parkos, C.A., Nusrat, A., 2016. Inflammation and the intestinal barrier: leukocyte-epithelial cell interactions, cell junction remodeling, and mucosal repair. Gastroenterology 151, 616–632.
[96] He, L.W., Meng, Q.X., Li, D.Y., Zhang, Y.W., Ren, L.P., 2015. Influence of feeding alternative fiber sources on the gastrointestinal fermentation, digestive enzyme activities and mucosa morphology of growing Greylag geese. Poult Sci 94, 2464–2471.
[97] Amevor, F.K., Cui, Z., Du, X., Ning, Z., Deng, X., Xu, D., et al., 2022. Supplementation of dietary quercetin and vitamin E promotes the intestinal structure and immune barrier integrity in aged breeder hens. Front Immunol 13, 860889.
[98] Singh, R., Chandrashekharappa, S., Bodduluri, S.R., Baby, B.V., Hegde, B., Kotla, N.G., et al., 2019. Enhancement of the gut barrier integrity by a microbial metabolite through the Nrf2 pathway. Nat Commun 10, 89.
[99] Santos-Moriano, P., Fernandez-Arrojo, L., Mengibar, M., Belmonte-Reche, E., Peñalver, P., Acosta, F., et al., 2018. Enzymatic production of fully deacetylated chitooligosaccharides and their neuroprotective and anti-inflammatory properties. Biocatal Biotransform 36, 57–67.
[100] Xing, R., Liu, Y., Li, K., Yu, H., Liu, S., Yang, Y., et al., 2017. Monomer composition of chitooligosaccharides obtained by different degradation methods

and their effects on immunomodulatory activities. Carbohydr Polym 157, 1288–1297.
[101] Zhang, H., Zhang, Y., Huang, Y., Wu, L., Guo, Q., Wang, Q., et al., 2021. Interaction between bovine serum albumin and chitooligosaccharides: I. Molecular mechanism. Food Chem 358, 129853.
[102] Fan, S., Li, Z., Fan, C., Chen, J., Huang, H., Chen, G., et al., 2022. Fast-thermoresponsive carboxylated carbon nanotube/chitosan aerogels with switchable wettability for oil/water separation. J Hazard Mater 433, 128808.
[103] Matich, E.K., Chavez Soria, N.G., Aga, D.S., Atilla-Gokcumen, G.E., 2019. Applications of metabolomics in assessing ecological effects of emerging contaminants and pollutants on plants. J Hazard Mater 373, 527–535.
[104] Zhang, Y., Ji, X., Ku, T., Li, B., Li, G., Sang, N., 2019. Ambient fine particulate matter exposure induces cardiac functional injury and metabolite alterations in middle-aged female mice. Environ Pollut 248, 121–132.
[105] Ning, X., Li, B., Ku, T., Guo, L., Li, G., Sang, N., 2018. Comprehensive hippocampal metabolite responses to PM2.5 in young mice. Ecotoxicol Environ Saf 165, 36–43.
[106] Wang, B., Tsakiridis, E.E., Zhang, S., Llanos, A., Desjardins, E.M., Yabut, J.M., et al., 2021. The pesticide chlorpyrifos promotes obesity by inhibiting diet-induced thermogenesis in brown adipose tissue. Nat Commun 12.
[107] Maya-Lopez, M., Rubio-Lopez, L.C., Rodriguez-Alvarez, I.V., Orduno-Piceno, J., Flores-Valdivia, Y., Colonnello, A., et al., 2020. Receptor-mediated mechanism participates in the neuroprotective effects of oleamide against excitotoxic damage in rat brain synaptosomes and cortical slices. Neurotox Res 37, 126–135.
[108] Alegiry, M.H., El Omri, A., Bayoumi, A.A., Alomar, M.Y., Rather, I.A., Sabir, J.S. M., 2022. Antidepressant-like effect of traditional medicinal plant Carthamus tinctorius in mice model through neuro-behavioral tests and transcriptomic approach. Appl Sci 12.
[109] Machado, M., Serra, C.R., Oliva-Teles, A., Costas, B., 2021. Methionine and tryptophan play different modulatory roles in the European Seabass (*Dicentrarchus labrax*) innate immune response and apoptosis signaling-an in vitro study. Front Immunol 12, 660448.
[110] de Oliveira, J., Farias, H.R., Streck, E.L., 2021. Experimental evidence of tyrosine neurotoxicity: focus on mitochondrial dysfunction. Metab Brain Dis 36, 1673–1685.
[111] Wang, C., Wang, F., Wang, Y., Fu, L., 2022. D-tryptophan triggered epithelial-mesenchymal transition by activating TGF-β signaling pathway. Food Sci Hum Wellness 11, 1215–1221.
[112] Munn, A.L., Weaver, A.C., van Wettere, W., 2021. Supplementary tryptophan fed to sows prior to and after farrowing to improve piglet growth and survival. Anim Open Access J MDPI 11.
[113] Henry, M., Shoveller, A.K., O'Sullivan, T.L., Niel, L., Friendship, R., 2022. Effect of varying levels of dietary tryptophan on aggression and abnormal behavior in growing pigs. Front Vet Sci 9, 849970.
[114] Wang, Y., Jin, C., Wang, D., Zhou, J., Yang, G., Shao, K., et al., 2021. Effects of chlorothalonil, prochloraz and the combination on intestinal barrier function and glucolipid metabolism in the liver of mice. J Hazard Mater 410, 124639.
[115] Dai, S., Wang, Z., Yang, Y., Du, P., Li, X., 2022. PM2.5 induced weight loss of mice through altering the intestinal microenvironment: Mucus barrier, gut microbiota, and metabolic profiling. J Hazard Mater 431, 128653.
[116] Li, J., Pang, B., Shao, D., Jiang, C., Hu, X., Shi, J., 2020. Artemisia sphaerocephala Krasch polysaccharide mediates lipid metabolism and metabolic endotoxaemia in associated with the modulation of gut microbiota in diet-induced obese mice. Int J Biol Macromol 147, 1008–1017.
[117] Wang, Y., Tang, C., Tang, Y., Yin, H., Liu, X., 2020. Capsaicin has an anti-obesity effect through alterations in gut microbiota populations and short-chain fatty acid concentrations. Food Nutr Res 64.
[118] Yoo, S.R., Kim, Y.J., Park, D.Y., Jung, U.J., Jeon, S.M., Ahn, Y.T., et al., 2013. Probiotics L. plantarum and L. curvatus in combination alter hepatic lipid metabolism and suppress diet-Induced obesity. Obesity 21, 2571–2578.
[119] Li, W.J., Zhang, L., Wu, H.X., Li, M., Wang, T., Zhang, W.B., et al., 2022. Intestinal microbiota mediates gossypol-induced intestinal inflammation, oxidative stress, and apoptosis in fish. J Agric Food Chem 70, 6688–6697.
[120] Li, D., Miao, J., Pan, L., Zhou, Y., Gao, Z., Yang, Y., et al., 2021. Impacts of benzo (a)pyrene exposure on scallop (Chlamys farreri) gut health and gut microbiota composition. Sci Total Environ 799, 149471.
[121] Clavel, T., Charrier, C., Wenning, M., Haller, D., 2013. Parvibacter caecicola gen. nov., sp. nov., a bacterium of the family Coriobacteriaceae isolated from the caecum of a mouse. Int J Syst Evol Microbiol 63, 2642–2648.
[122] Lynch, K.M., Lucid, A., Arendt, E.K., Sleator, R.D., Lucey, B., Coffey, A., 2015. Genomics of Weissella cibaria with an examination of its metabolic traits. Microbiology 161, 914–930.
[123] Stoll, D.A., Danylec, N., Soukup, S.T., Hetzer, B., Kulling, S.E., Huch, M., 2021. Adlercreutzia rubneri sp. nov., a resveratrol-metabolizing bacterium isolated from human faeces and emended description of the genus *Adlercreutzia*. Int J Syst Evol Microbiol 71.
[124] Zhao, T., Zhong, S., Xu, J., Jiao, W., Liu, W., Huang, L., et al., 2022. PAYCS alleviates scopolamine-induced memory deficits in mice by reducing oxidative and inflammatory stress and modulation of gut microbiota-fecal metabolites-brain neurotransmitter axis. J Agric Food Chem 70, 2864–2875.
[125] Senatore, G., Mastroleo, F., Leys, N., Mauriello, G., 2020. Growth of Lactobacillus reuteri DSM17938 under two simulated microgravity systems: changes in reuterin production, gastrointestinal passage resistance, and stress genes expression response. Astrobiology 20, 1–14.